The Astrophysical Journal, 574:1021–1038, 2002 August 1

THE STRUCTURE AND EVOLUTION OF A SIGMOIDAL ACTIVE REGION

S. E. Gibson,[1] L. Fletcher,[2] G. Del Zanna,[3] C. D. Pike,[4] H. E. Mason,[3] C. H. Mandrini,[5] P. Démoulin,[6] H. Gilbert,[1] J. Burkepile,[1] T. Holzer,[1] D. Alexander,[7] Y. Liu,[8] N. Nitta,[7] J. Qiu,[9] B. Schmieder,[6] and B. J. Thompson[10]

Received 2001 October 17; accepted 2002 April 5

ABSTRACT

Solar coronal sigmoidal active regions have been shown to be precursors to some coronal mass ejections. Sigmoids, or S-shaped structures, may be indicators of twisted or helical magnetic structures, having an increased likelihood of eruption. We present here an analysis of a sigmoidal region's three-dimensional structure and how it evolves in relation to its eruptive dynamics. We use data taken during a recent study of a sigmoidal active region passing across the solar disk (an element of the third Whole Sun Month campaign). While S-shaped structures are generally observed in soft X-ray (SXR) emission, the observations that we present demonstrate their visibility at a range of wavelengths including those showing an associated sigmoidal filament. We examine the relationship between the S-shaped structures seen in SXR and those seen in cooler lines in order to probe the sigmoidal region's three-dimensional density and temperature structure. We also consider magnetic field observations and extrapolations in relation to these coronal structures. We present an interpretation of the disk passage of the sigmoidal region, in terms of a twisted magnetic flux rope that emerges into and equilibrates with overlying coronal magnetic field structures, which explains many of the key observed aspects of the region's structure and evolution. In particular, the evolving flux rope interpretation provides insight into why and how the region moves between active and quiescent phases, how the region's sigmoidicity is maintained during its evolution, and under what circumstances sigmoidal structures are apparent at a range of wavelengths.

Subject headings: MHD — Sun: activity — Sun: magnetic fields

On-line material: color figures

1. INTRODUCTION

Coronal mass ejections (CMEs) are fascinating demonstrations of the complexity and power of magnetohydrodynamic processes at the Sun. "Sigmoids," the name given to S-shaped (or inverse-S–shaped) coronal active regions as seen in soft X-ray emission, have been shown to be precursors to CMEs (Manoharan et al. 1996; Hudson et al. 1998; Rust & Kumar 1996; Sterling & Hudson 1997; Pevtsov & Canfield 1999) and statistically more likely to erupt (Canfield, Hudson, & McKenzie 1999). Interestingly, although these regions can be sites of greater than usual activity, the overall S or inverse-S shape can survive for days or weeks. Thus, the basic configuration of the sigmoidal active region is almost paradoxically stable.

Many of the analyses to date have concentrated on X-ray observations of sigmoids, often in relation to magnetic field observations, because X-ray is the frequency regime where sigmoids are most commonly monitored (Hudson et al. 1998; Sterling & Hudson 1997; Canfield et al. 1999; López Fuentes et al. 2000; Moore et al. 2001). Hα observations of sigmoidal filaments have also been studied (Rust & Kumar 1996; Pevtsov, Canfield, & Zirin 1996; Lites & Low 1997; Gibson & Low 2000; Pevtsov 2002). However, these two extremes show only the hottest and coldest material associated with the sigmoidal region. A multiwavelength study is required to probe the entire structure and to consider how the sigmoid plasma relates to its underlying magnetic field. A few such detailed analyses of specific sigmoid-related flares and CMEs have recently been done (Sterling et al. 2000; Zarro et al 1999; Wang et al. 2000; Aurass et al. 1997), as well as surveys of the general characteristics of sigmoids at a range of temperatures (Gibson et al. 1999a; Glover et al. 2001).

In 1999 August, a multiwavelength analysis of a sigmoidal active region was run, as part of the third Whole Sun Month (WSM3) campaign. Observations included data from the *Solar and Heliospheric Observatory* (*SOHO*), *Transition Region and Coronal Explorer* (*TRACE*), *Yohkoh*, Big Bear Solar Observatory (BBSO), Meudon Observatory, and Mauna Loa Solar Observatory (MLSO) telescopes. The Whole Sun Month campaigns have provided excellent opportunities for observers and modelers to work together to describe the three-dimensional morphology, plasma properties, and magnetic field of the global corona and to connect these structurally to in situ observations (Biesecker et al. 1999; Galvin & Kohl 1999; Gibson et al. 1999b). The WSM3 campaign studied the global corona during the ascending phase of the solar cycle and consisted of several Joint Observing Programs (JOPs), among them the sigmoi-

[1] HAO/NCAR, P.O. Box 3000, Boulder, CO 80307.
[2] Department of Physics and Astronomy, University of Glasgow, Glasgow G12 8QQ, UK.
[3] DAMTP, University of Cambridge, Silver Street, Cambridge CB3 9EW, UK.
[4] Rutherford Appleton Laboratory, Chilton, Didcot, Oxfordshire OX11 0QX, UK.
[5] Instituto de Astronomía y Física del Espacio, Casilla de Correo 67, Sucursal 28, Buenos Aires 1428, Argentina.
[6] Observatoire de Paris, section Meudon, DASOP, URA 2080 (CNRS), F-92195 Meudon Principal Cedex, France.
[7] Lockheed-Martin Solar and Astrophysics Laboratory, Org L9-41/B252, 3251 Hanover Street, Palo Alto, CA 94304.
[8] HEPL/CSSA, Stanford University, Stanford, CA 944305-4085.
[9] Big Bear Solar Observatory, New Jersey Institute of Technology, 40386 North Shore Lane, Big Bear City, CA 92314-9672.
[10] NASA Goddard Space Flight Center, Code 682, Greenbelt, MD 20771.

dal active region study (*SOHO*/*TRACE* JOP 106). This JOP provided the first opportunity to study a sigmoidal region in depth and at multiple wavelengths as it crossed the solar disk. Thus, we were able to analyze its structure from multiple lines of sight and temperature regimes and study how its evolution related to dynamic events on the Sun during its passage.

Section 2 of this paper will describe observations of how the sigmoidal region evolved and exhibited coronal activity as it crossed the disk. Details of the activity in the region are specified in the time line of Table 1. Section 3 will present analyses of the physical structure (magnetic field, density, temperature, and velocity) of the region. The large volume of detailed data obtained in the campaign covers nearly 2 weeks and a wide range of frequencies. Therefore, in order to make sense of what otherwise might be an overwhelming amount of observational information, we summarize some questions raised by the observations at the end of each of these sections. Moreover, in § 4 we present a possible theoretical interpretation of the observed sigmoid structure and evolution, in terms of a magnetic flux rope emerging into and equilibrating with the coronal environment. In particular, we will consider the observed behavior of the region, where first the sigmoidal region is active, with multiple flares and associated eruptions, then it moves on to a relatively quiescent stage, and then destabilizes amid emerging magnetic flux and further X-ray activity and eruptions. Such behavior is consistent with a flux rope that emerges, interacts with its external environment until it reaches a metastable equilibrium, is destabilized by new emerging magnetic flux and other changes in its environment, and again goes through the process of equilibrating via flaring and eruptions and possibly a partial ejection of the rope itself. In § 5 we present our conclusions.

2. EVOLUTION OF THE SIGMOIDAL ACTIVE REGION

2.1. *Summary of Activity Associated with the Sigmoidal Region*

Extensive activity was associated with our sigmoidal region during its passage across the solar disk. Identified as NOAA AR 8668, it appeared at the limb of the northeast quadrant approximately on 1999 August 12, had a large CME associated with it on August 14, and became identifiable as an inverse-S–oriented sigmoid on August 16 using X-ray images taken by the *Yohkoh*/Soft X-Ray Telescope (SXT) satellite. The WSM3 streamer study (*SOHO*/*TRACE* JOP 76) immediately targeted a neighboring streamer in the northeast as a good candidate for eruption, and indeed, on August 17 the streamer with its associated polar crown filament blew out in a coronal mass ejection. This CME was accompanied by flaring in AR 8668 (we will discuss the relationship between the CME and AR 8668 in more detail below). These flares were part of a series of B- and C-class flares observed in AR 8668 between August 16 and 17 (R. C. Canfield et al. 2002, in preparation). An inverse-S–shaped filament, clearly visible in Hα and more or less aligned with the X-ray sigmoid, formed in stages along the neutral line starting on August 16 (Figs. 1*a* and 1*b*), was at its largest and most continuously apparent on August 18 and most of August 19 (Fig. 1*c*), underwent disappearance as new flux emerged near its midpoint between August 20 and 21 (Figs. 1*d* and 1*e*), and then may have partially reestablished itself along portions of the significantly altered neutral line between August 22 and 24 (Fig. 1*f*). On August 21 a small flarelike brightening event showed sigmoidal structure at a range of wavelengths (Figs. 2 and 3; note that throughout this paper, we will refer to a flare only if it is *GOES* classified—otherwise, we will refer to brightenings or flarelike brightenings). Finally, a jet that may have been associated with this sigmoidal region occurred on August 26, when AR 8668 was at the west limb (Y.-K. Ko et al. 2002, in preparation).

Throughout the sigmoidal region's disk passage, X-ray loops continued to reform into identifiable inverse-S shapes between events until projection effects made such identification impossible. Likewise, the sigmoidal filament appeared and disappeared in Hα, lying along the underlying inverse-S–shaped neutral line (although after the new magnetic flux emerged, the neutral line's inverse-S shape was essentially disrupted). One of the questions we wished to address with our multiwavelength study was to what extent sigmoidal structures became visible in temperatures other than the very hot (3–5 million K) X-ray loops or the cold (5000–10,000 K) Hα filament. A preliminary survey of *SOHO*/Coronal Diagnostics Spectrometer (CDS; Harrison et al. 1995) observations of regions designated sigmoidal by X-ray observations (Canfield et al. 1999) found evidence for S-shaped structures at a range of temperatures (20,000 to 1 million K or He I to Si XII) (Gibson et al. 1999a). However, observations of the disk passage of AR 8668 demonstrated that our sigmoid was not obvious at most temperatures, with the notable exception of the small inverse-S brightening of August 21, which was visible in emission at a range of temperatures (Figs. 2 and 3). This multiwavelength brightening will be discussed further in § 3.

2.2. *Details of Sigmoidal Region Evolution*

In order to better interpret the observations, we will now present details of the sigmoidal region's evolution for four key time periods: (1) the "active" period of multiple flares and the northeast CME (August 16–17), (2) the relatively quiescent period of the "stable" sigmoidal filament (August 18–19), (3) the period of filament disintegration and further CME/X-ray activity (August 20–21), and finally (4) the observations of what remained of the sigmoidal region as it approached the west limb (August 22–26). A time line of observations can be found in Table 1.

1999 August 16 and 17: Flares and filament formation.—Prior to and early on August 16, to the extent establishable using near-limb observations, some filament material was intermittently visible in both the northern and the southern portions of an inverse-S–shaped filament channel, although often not at the same time. The appearance of the southern part of the inverse-S–shaped filament on the afternoon of August 16 was accompanied by flaring (*GOES* C class) along the filament channel (Fig. 1*a*; note that the large cusp seen in X-rays in the southern part of the sigmoid on August 16 is associated with earlier activity, possibly the CME of August 14). Meanwhile, filament material in the northern portion of the inverse-S–shaped filament channel was intermittently visible and appeared to erupt (or at least disappear) at least once (see Table 1). During this activity the southern portion of the filament did not greatly change. On August 17, the northern extension of the filament appeared

TABLE 1

TIME LINE FOR DISK PASSAGE OF SIGMOIDAL NOAA AR 8668 FROM 1999 AUGUST 13 TO AUGUST 26

Days	Hours (UT)	Events
1999 Aug 13		**No** relevant **CMEs** or **flares**
1999 Aug 14	05:24	EIT (195 Å) **dimming** in AR 8668
	06:30	LASCO C2 (white light) **CME** in northeast
	10:12	EIT bright **loops** in AR 8668
	11:58	SXT (X-ray) sees beginning of **flare** in AR 8668
	11:58–12:15 (peak 12:10)	*GOES* C7.2 **flare** in AR 8668
	12:12	EIT sees **flare** in AR 8668
	17:52	Beginnings of **cusp** in southern part of AR 8668 visible to SXT
1999 Aug 15	12:53–13:11 (peak 13:00)	*GOES* B7.2 **flare** in AR 8668
		No relevant white light **CMEs**
1999 Aug 16		Material flowing out at east limb in white light (LASCO C2–C3) but **no CME** obviously associated with activity in AR 8668
	00:18–00:48 (peak 00:34)	*GOES* C1.3 **flare** in AR 8668
	08:54	Meudon (Hα): some **filament** material in southern portion of sigmoidal filament channel
	14:00–17:00	**Surges** of material in the vicinity of AR 8668, visible in EIT, BBSO (Hα on-disk), and MLSO/PICS (Hα limb); sigmoidal **filament** intermittently visible, mostly in the southern part
	16:37–16:53 (peak 16:42)	*GOES* B8.1 **flare** in AR 8668, visible also in BBSO; **brightening** along sigmoidal filament channel
	20:23–20:35 (peak 20:29)	*GOES* C1.2 **flare** in AR 8668, visible also in BBSO, apparently localized in sunspot to the right of sigmoidal filament channel
	20:49–22:34	BBSO observations show northern portion of sigmoidal **filament** apparently **erupting**, while southern part remains
1999 Aug 17	03:18–03:47 (peak 03:34)	*GOES* B9.5 **flare** in AR 8668
	03:24	EIT **dimming** north of AR 8668
	12:32–13:57 (peak 13:23)	*GOES* C2.6 **flare** in AR 8668
	12:47	EIT **brightening** along sigmoidal filament channel
	13:13	EIT **dimming** just northeast of AR 8668
	13:31	LASCO C2 **CME** in northeast streamer
	14:12	EIT northeast **streamer deflection**
	14:28–17:54 (peak 16:02)	*GOES* C5.9 **flare** in AR 8668
	14:34	SXT **cusp** above northern portion of filament channel
	14:38	EIT and BBSO **two-ribbon flare** visible to northeast of AR 8668
	14:44	BBSO and EIT **polar crown filament erupts** north of AR 8668
	14:38–18:02	BBSO still sees southern portion of **filament**, and northern portion becomes visible
	16:00	EIT **postflare loops** along and just northeast of AR 8668
	Aug 17 15:00–Aug 18 15:00	MDI (photospheric magnetic field) sees **flux cancellation** near midpoint of sigmoidal filament channel
1999 Aug 18		**No** relevant white light **CMEs or flares**
		Filament material visible along entire length of sigmoidal filament channel; **some motion** observed in southern portion by BBSO and **some brightening** observed in southern loops by EIT and SXT throughout the day
1999 Aug 19		Full clear sigmoidal **filament** along entire length of sigmoidal filament channel visible throughout the day in BBSO and Meudon; although there is some faint material moving outward in all directions during the day visible in LASCO C2–C3, there is no clear halo CME relatable to AR 8668
	22:00	**Motion** in southern part of **filament** seen by EIT and BBSO
1999 Aug 20		**No** obvious white light **CME** associated with activity in AR 8668
	06:33	Full sigmoidal **filament** visible in Meudon
	07:36	EIT sees **dimming** in AR 8668
	08:20	Southern part of **filament brightens** and **disappears** (Meudon; *TRACE* 171, 195, 284 Å; EIT)
	14:47	EIT sees **postflare-like loops** in AR 8668
	14:59	BBSO: southern part of **filament** gone (or very faint)
1999 Aug 21		Beginning around 08:00 UT and throughout the day, MDI sees **emerging magnetic flux** near the midpoint of the sigmoidal filament channel
	12:30–13:30	*TRACE* sees brightening in EFR and to the north and motion of northern part of filament; Meudon sees northern part of filament disappearing (observations end at 13:30 UT)
	14:10–14:50	*TRACE* sees **brightening** along northern part of filament channel and at EFR
	13:50	LASCO C2 slow **CME** in northwest quadrant
		No obvious **dimming** on disk, as seen by EIT
	14:53	BBSO: sigmoidal **filament mostly gone** (faint trace of southern filament remains); **arched filament system** visible across emerging magnetic flux
	17:36–18:47	**Subsigmoid brightening** visible in *TRACE*, CDS (He I, O V, Mg X, Si XII, Fe XIX), EIT, and SXT
	21:00	BBSO sees remaining wisp of southern **filament disappear**
1999 Aug 22		No obvious **flares or CMEs** associated with AR 8668
		Emerging magnetic flux continues to grow (MDI), along with **arched filament system** (BBSO)

TABLE 1—*Continued*

Days	Hours (UT)	Events
		Some **filament** material lies in southern portion of region (but difficult to tell if it is a reformation of our original filament or an independent structure)
		Some material also visible in northern part of region (BBSO, Helio Research Hα)
		Emerging flux region splits the north from the south; no longer a continuous sigmoid filament channel (BBSO)
1999 Aug 23		**No** obvious **flares or CMEs** associated with AR 8668
		Hα **filament** observations (BBSO) similar to Aug 22
1999 Aug 24		**No** obvious **flares or CMEs** associated with AR 8668
1999 Aug 25		**No** obvious **flares or CMEs** associated with AR 8668
	09:17	Meudon **filament** in southern part of region visible
	14:38/54	Helio/BBSO **filament** in southern part of region gone
	21:18	**Jet and CME** in the vicinity of AR 8668 seen in many wavelengths (LASCO, CDS, UVCS [UV], EIT, *TRACE*, MLSO/PICS, MLSO/CHIP [10830 Å]

NOTES.—Multiple data sets are represented in this table; in general, these do not have 24 hr coverage (although *SOHO*/EIT and *SOHO*/LASCO data did cover 24 hr, and we examined these for relevant activity). Necessarily, therefore, not all activity during the time period is represented, but specifics for well-observed activity are given for the purpose of reference within this paper. We have erred on the side of overinclusion, so that any activity potentially relevant to AR 8668 is cited. The wavelength of observations is listed for each instrument the first time it appears in the time line. Key events are given in bold for ease of reading.

to stabilize after an initial C-class flare and during a subsequent C-class flare (which led to the small cusp in the northern part of the X-ray sigmoid visible in Fig. 1*b*). Interestingly, *SOHO*/Michelson Doppler Imager (MDI) observed a magnetic flux cancellation near the midpoint between the northern and southern portions of the inverse-S–shaped filament, just as the northern portion of the filament was apparently stabilizing (Fig. 4).

The activity on August 17 was not limited to the immediate vicinity of our sigmoidal region. The first C-class flare occurred along the S-shaped neutral line and was quickly followed by (1) a dimming as observed by *SOHO*/EUV Imaging Telescope (EIT) extending up to the northeast of AR 8668 (see Thompson et al. 1999 for a discussion of *SOHO*/EIT dimmings and their relation to CMEs), (2) a streamer deflection on the northeast limb observed by *SOHO*/EIT and the appearance of a CME in *SOHO*/Large Angle and Spectrometric Coronagraph (LASCO) C2 white light observations, (3) a second GOES C-class flare in AR 8668 accompanied by a *Yohkoh*/SXT cusp and a two-ribbon flare visible in Hα and later by postflare loops visible in *SOHO*/EIT and *Yohkoh*/SXT, and (4) the launching of a polar crown filament to the north of AR 8668. In the midst of the later part of this activity, the northern portion of the sigmoidal filament became steadily more visible, as indicated by BBSO Hα observations beginning just after the second C-class flare. Note that Hα data (when it was available) indicated that the southern portion of the filament remained visible throughout the activity of August 17.[11]

August 18–19: Growth of the filament.—After the flare of August 16 for the southern portion and the flares on August 17 for the northern portion, each portion had a temporarily quiescent phase, so that for much of August 18 and 19 a filament was visible along the entire inverse-S–shaped neutral line (Fig. 1*c*). Incomplete Hα data coverage necessarily qualifies this conclusion (see Table 1 for specific times of coverage); however, continuous *SOHO*/EIT and *SOHO*/LASCO data for August 18–19 do not indicate any obvious white light CMEs or large flares associated with the region, and also no new *Yohkoh*/SXT cusps appeared in AR 8668 in this time period. There was some brightening in the southern part of the sigmoid seen by *SOHO*/EIT and *Yohkoh*/SXT, and this was accompanied by some evolution of the southern filament as observed in Hα, so that the southern portion of the filament appeared fairly thin for parts of August 18. By August 19, however, the southern portion had grown to its greatest apparent width, and a full, clear sigmoid outlining the entire inverse S was visible in Hα observations (see Fig. 1*c*). We also note that while the Hα sigmoidal filament had its most obvious inverse-S shape during this time, the X-ray sigmoid was less apparent, with mostly the fat southern loops evident (Fig. 1*c*).

August 20–21: Filament disintegration and eruption.—Very late on August 19, the southern portion of the filament was observed by BBSO to destabilize and lose some of its material, and in the morning of August 20, Meudon Hα observations indicated that the southern portion of the filament disappeared entirely. *TRACE* observations showed movement of filament material, apparently up to the northeast, and *SOHO*/EIT saw a dimming, high-temperature flarelike brightening (which nonetheless did not have a *GOES* signature) and a set of loops suggestive of postflare loops that may have been associated with the filament disappearance (see Table 1 for specific times). However, no cusps in *Yohkoh*/SXT appeared, and no white light CMEs were observed that could be definitely associated with the filament disappearance. Therefore, it is impossible to conclude for certain whether filament material was bodily ejected. If it was, it is likely it was only a partial ejection of the flux rope, however, since a faint filament could be seen in the southern portion of the inverse-S–shaped filament channel later in the day (see Fig. 1*d*; also see Tang 1986). Note that the northern portion of the sigmoidal filament remained basically intact throughout the disappearance of the southern part.

On the morning of August 21, *SOHO*/MDI observed magnetic flux emerging at more or less the same filament midpoint as the magnetic flux cancellation of August 17.

[11] See Table 1 for specifics on the times of these observations and http://www.hao.ucar.edu/~sgibson/SIGMOID for EIT movies illustrating the spatial and temporal connections between AR 8668 and the CME-related activity.

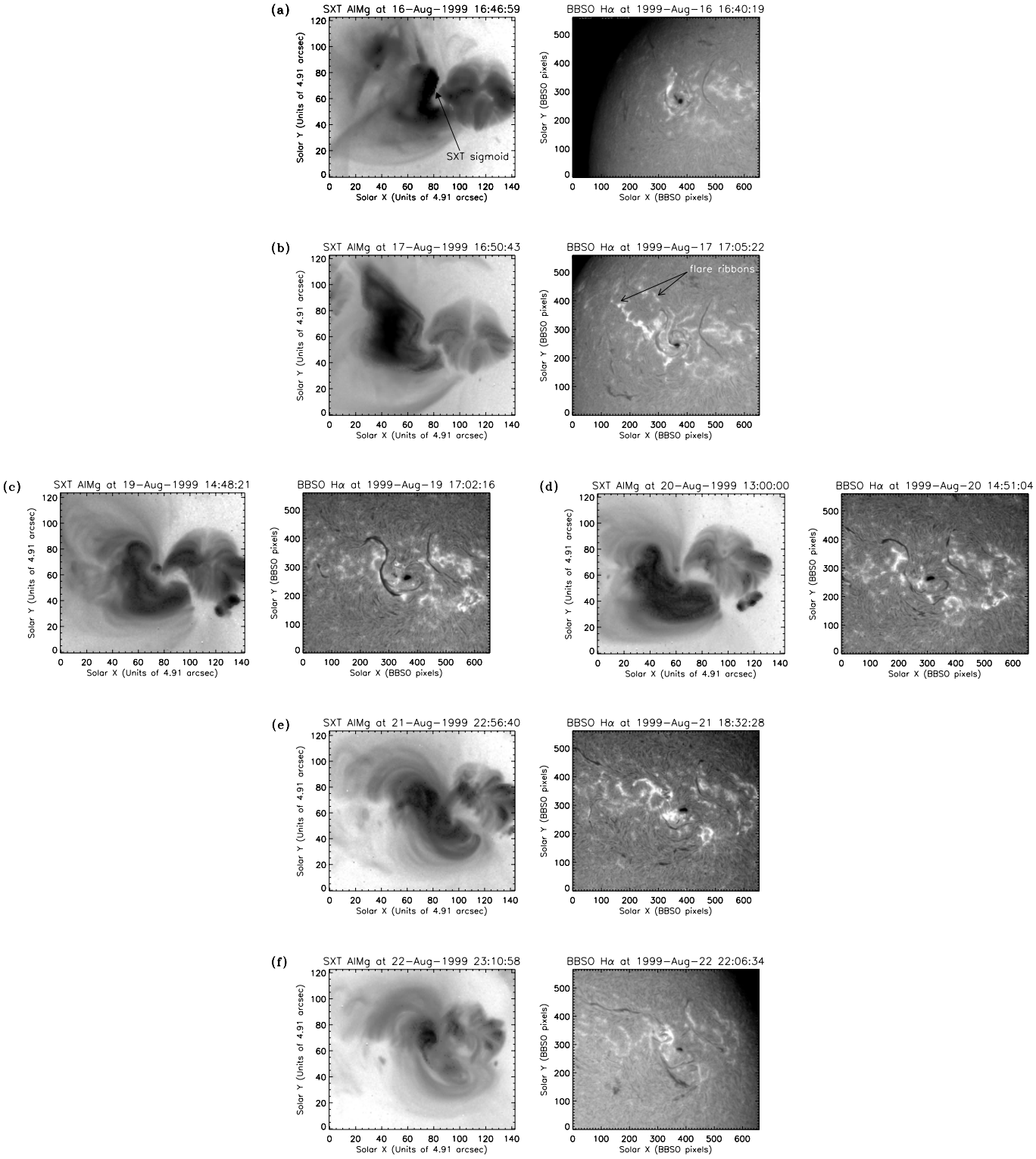

FIG. 1.—*Yohkoh*/SXT X-ray (*left columns*; inverted color table) and BBSO Hα (*right columns*) observations of sigmoidal AR 8668, 1999 August 16, 17, 19, 20, 21, and 22.

This flux emergence continued throughout the day and was also seen in BBSO Hα observations as an arched filament system (AFS) overlying the emerging flux region (EFR; see § 3.1 and Fig. 5). By the time of Figure 5, the northern part of the sigmoidal filament had vanished. Again, it is difficult to determine conclusively whether filament material was bodily ejected: although a white light CME was observed in the northwest quadrant, it appeared a little too soon (especially considering it was a slow CME) and was somewhat too narrow (considering the filament was near disk center) to be convincingly related to the filament disappearance, and so may have been an unrelated event originating on the

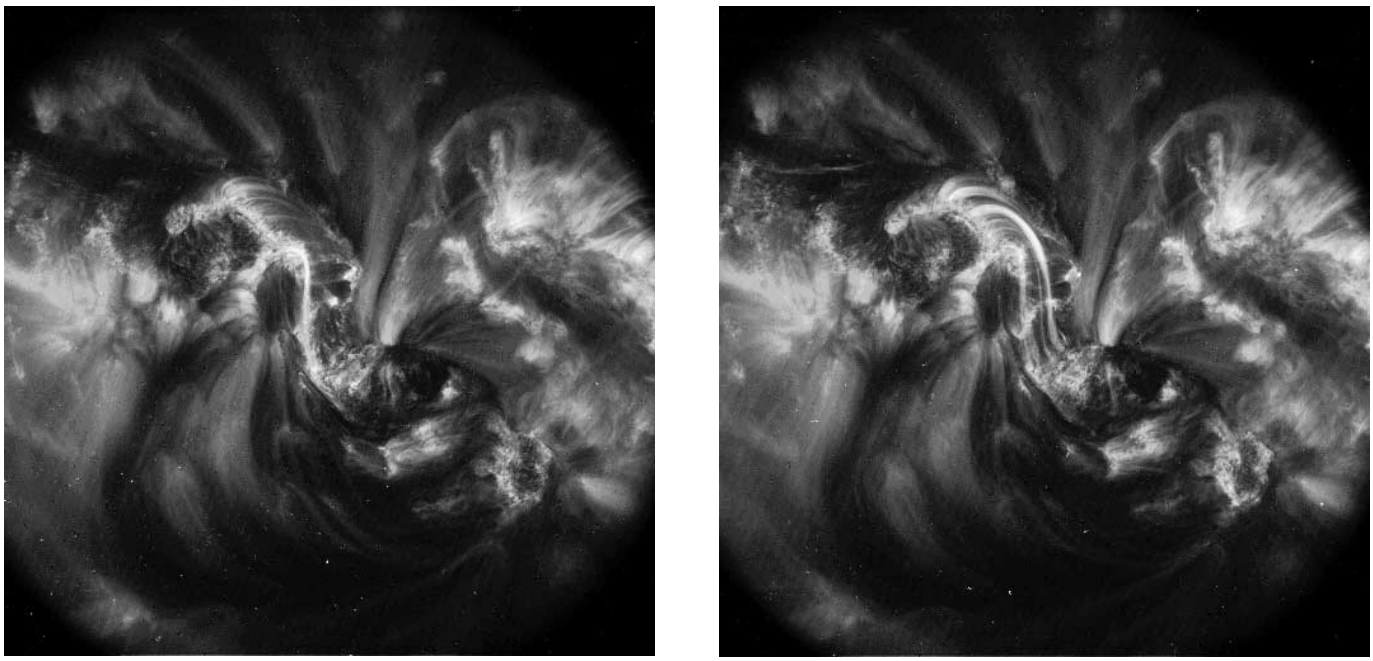

FIG. 2.—*TRACE* 195 Å emission of subsigmoid brightening on 1999 August 21 at 18:26 UT (*left panel*) and 18:51 UT (*right panel*). Note that these images are logarithmically scaled. [*See the electronic edition of the Journal for a color version of this figure.*]

back side of the Sun. Moreover, no obvious *SOHO*/EIT dimming could be seen (see Table 1 for specific times). As the day progressed, activity continued in the northern part of the sigmoidal region and included the brightening of an inverse-S–shaped substructure appearing in emission at a range of wavelengths. This will be discussed in more detail in § 3. Finally, we note that by the end of August 21, the sigmoidal filament was almost completely gone but the X-ray sigmoid was at its most evident (Fig. 1*e*).

August 22–26: Remains of the sigmoid.—As AR 8668 continued on its path to the west limb, it was somewhat more subdued. *Yohkoh*/SXT X-ray observations showed gener-

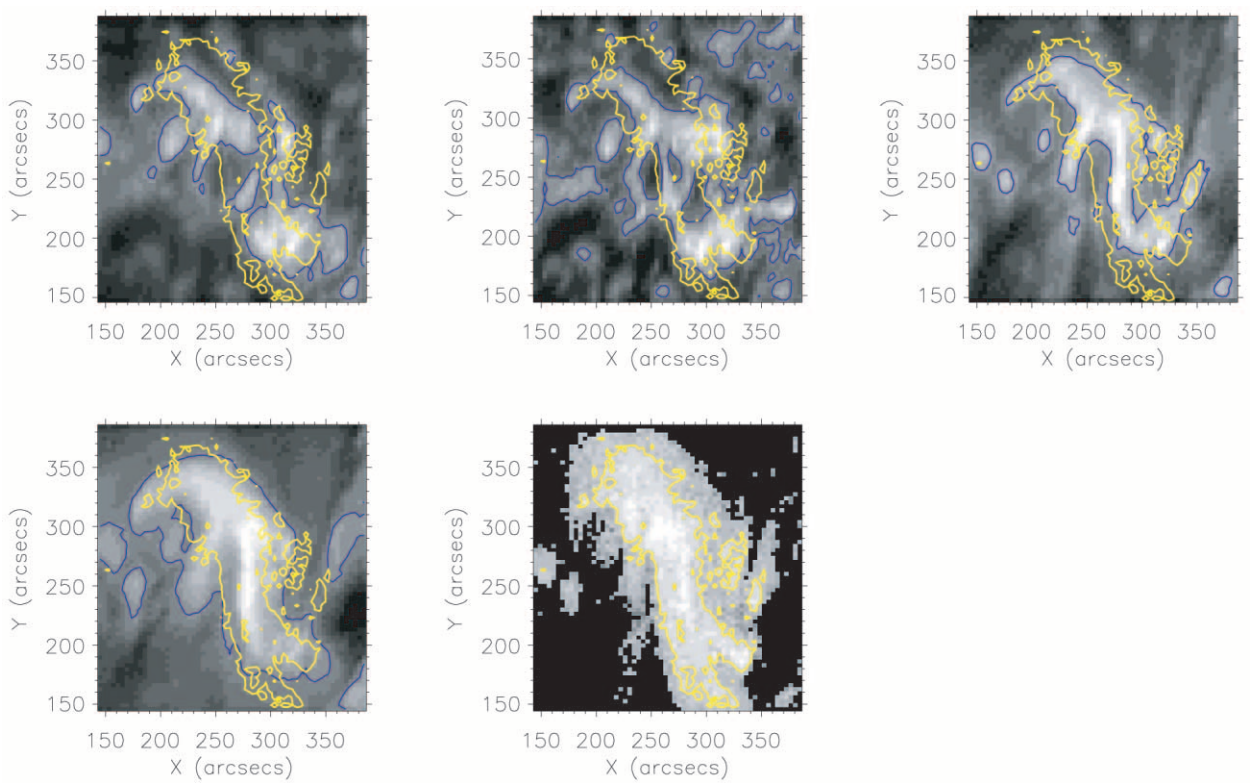

FIG. 3.—*SOHO*/CDS emission of subsigmoid brightening on 1999 August 21 at 18:21 UT, in (*clockwise from upper left*) He I, O V, Mg X, Fe XIX, and Si XII. Contours from each line are overlaid in blue; the additional thick yellow contours overlaid are from Fe XIX.

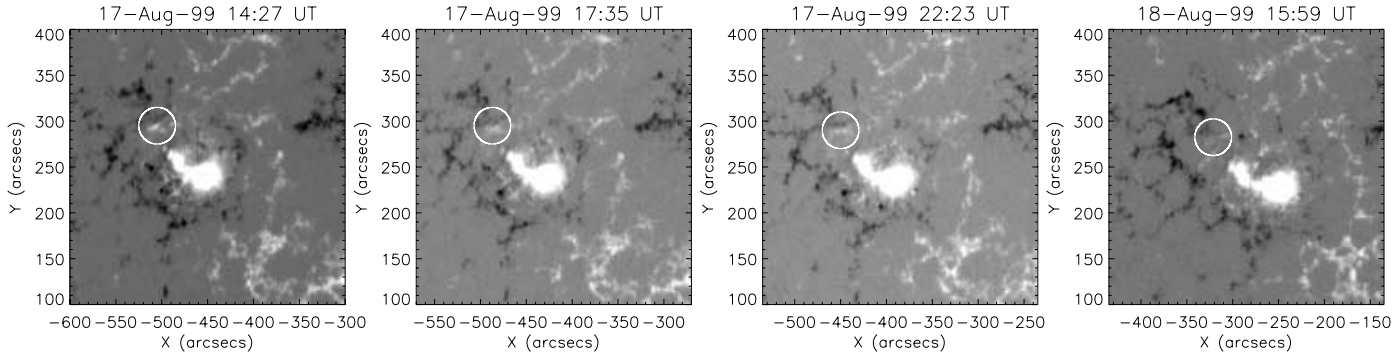

FIG. 4.—1999 August 17–18: MDI observations of magnetic field. Note the small white (positive) field to the northeast of the main white sunspot. Over the course of the first three images (August 17 14:27, 17:35, 22:23 UT) it disappears, with no trace remaining the following day (*right-hand image*; August 18 15:59 UT).

ally sigmoidal structure, although projection effects made such an identification increasingly difficult. Emerging magnetic flux continued to grow in the mid to northern part of the region, essentially severing the link between the northern and southern parts of the filament, so that a single inverse-S–shaped neutral line no longer existed. Filaments were intermittently apparent along neutral lines to the north and to the south of the EFR (Fig. 1*e*), and when the region was at the limb on August 26, a prominence was visible in emission, although because of projection effects it is difficult to say if this prominence was associated with our original flux rope or a neighboring magnetic structure.

On August 26 we witnessed the final chapter of our sigmoid observations, as a jetlike CME was observed at the west limb in white light and a range of wavelengths. Interestingly, velocity observations may indicate a twisting of the material in the jet (Y.-K. Ko et al. 2002, in preparation).

2.3. *Central Questions Raised by Observations of Sigmoid Evolution*

We will consider one possible interpretation of the sigmoidal region's evolution in § 4, but here let us first emphasize a few key questions that are immediately evident from the observations and that any interpretation would need to address.

1. Although there are several flares and eruptions, the region as observed in X-rays continually returns to a sigmoi-

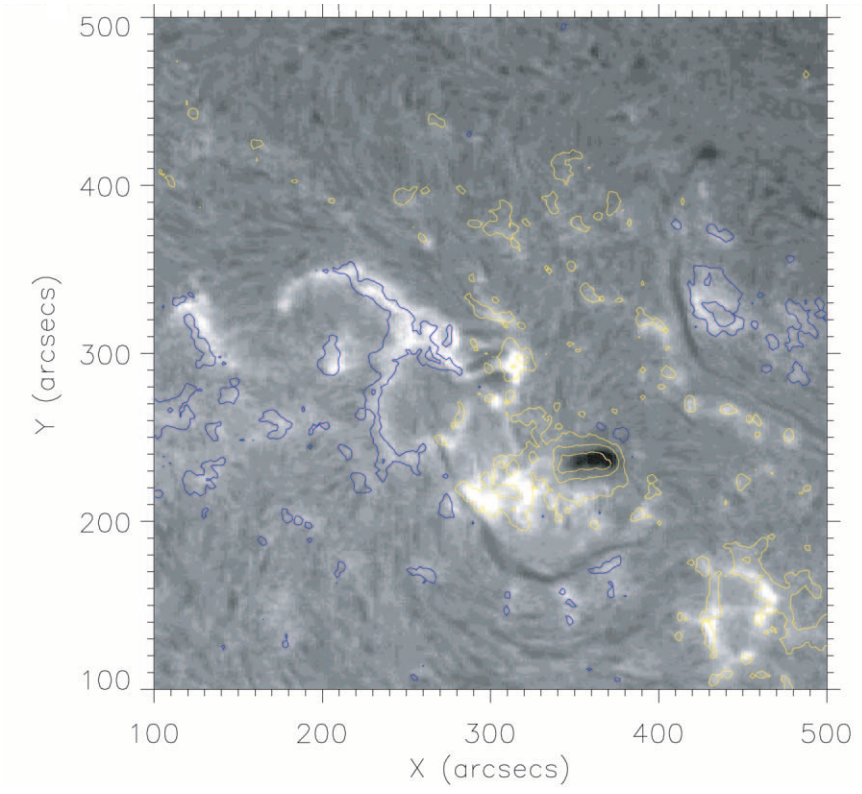

FIG. 5.—1999 August 21: BBSO Hα observations, with contours of MDI observations of magnetic field overlaid (*blue lines*: negative; *yellow lines*: positive). Note the EFR, which appears as a small magnetic bipole in the middle of the figure, with an AFS seen in Hα visible as dark horizontal lines connecting the ends of the magnetic bipole.

dal shape. What is the significance of this shape in terms of the energetics of the system, and why is it not permanently destroyed by all the activity?

2. The Hα filament in the region does not appear to be greatly disrupted by the flare of August 17, which temporarily transforms the X-ray sigmoid to a cusp shape; in fact, it becomes more clearly apparent during and after this activity (also see next question). Pevtsov (2002) showed several other cases of filaments associated with sigmoidal regions that were largely unperturbed by flares and apparent topological changes to the X-ray sigmoid. How is this possible? What does it imply about the relative locations of the filament and the X-ray sigmoid in the general magnetic structure of the region and their respective evolutions?

3. There is a general trend that when an inverse-S–shaped Hα filament is at its most visible, the X-ray sigmoid is not, and vice versa. In general, the X-ray sigmoid is brightest and best defined during or before periods of significant activity. The filament, on the other hand, is at its most complete inverse-S–shaped Hα structure during relatively quiescent times. Why does the sigmoidal region appear to move back and forth between active and quiescent periods in the manner observed?

4. The sigmoidal filament is observed in Hα to have its distinct northern and southern portions. The evolutions of these two portions have significant differences: they stabilize at different times and also disappear at different times. Moreover, the region between them is the site of both magnetic flux cancellation and emergence. Are these two portions separate magnetic structures or are they two parts of one larger element? And how is the evolution of the two portions of the filament related to the magnetic flux observations?

5. The August 17 observations of the activity in AR 8668 and of the CME to the northeast indicate both spatial and temporal connections between the two. How does the activity in the sigmoidal region relate to the larger scale activity of its external environment?

6. The last clear trace of the inverse-S–shaped filament disappeared from the northern portion after two notable changes in the region: first, the disappearance of the southern part of the filament during August 20, and second, the flux emergence between the northern and southern parts of the filament. Could these changes have contributed to a subsequent disappearance of the northern portion of the filament?

7. Finally, on August 21 an inverse-S–shaped region was apparent in many wavelengths, but for most wavelengths was localized to the northern part of the *Yohkoh*/SXT sigmoid. How is this substructure related to the sigmoidal region as a whole, and what caused its brightening?

In order to address the issue of this substructure and raise further key questions, we now turn to further observations and analysis of the three-dimensional structure of the sigmoidal region.

3. SIGMOID STRUCTURE

3.1. *Magnetic Complexity of NOAA AR 8668*

An interpretation of a sigmoidal active region as a single group of twisted or sheared field lines implies that these field lines should be rooted in a single magnetic bipole. By overlaying coronal structures on the observed photospheric field, we see that this was never the case for our sigmoidal region. Rather, two sets of loops end at two different positive poles: shorter loops connect to the northerly pole centered on the sunspot and longer loops connect to a more diffuse southerly pole (Fig. 6*a*). It is the longer loops that were generally identified as the X-ray sigmoid throughout its disk passage, although because of projection effects the X-ray sigmoid often was a superposition of both sets of loops. This was the case during the August 21 multiwavelength brightening (Fig. 6*b*). However, during this brightening the shorter loops were visible at a range of wavelengths (Figs. 3 and 7), while the longer loops were still clearly visible only in the very hot X-ray emission (Fig. 8). Also, the shorter loops manifested a distinctly sigmoidal appearance during the brightening (Fig. 2). For clarity and brevity, from here on we will refer to the sigmoid seen in the short loops as the subsigmoid and the original X-ray sigmoid as the supersigmoid.

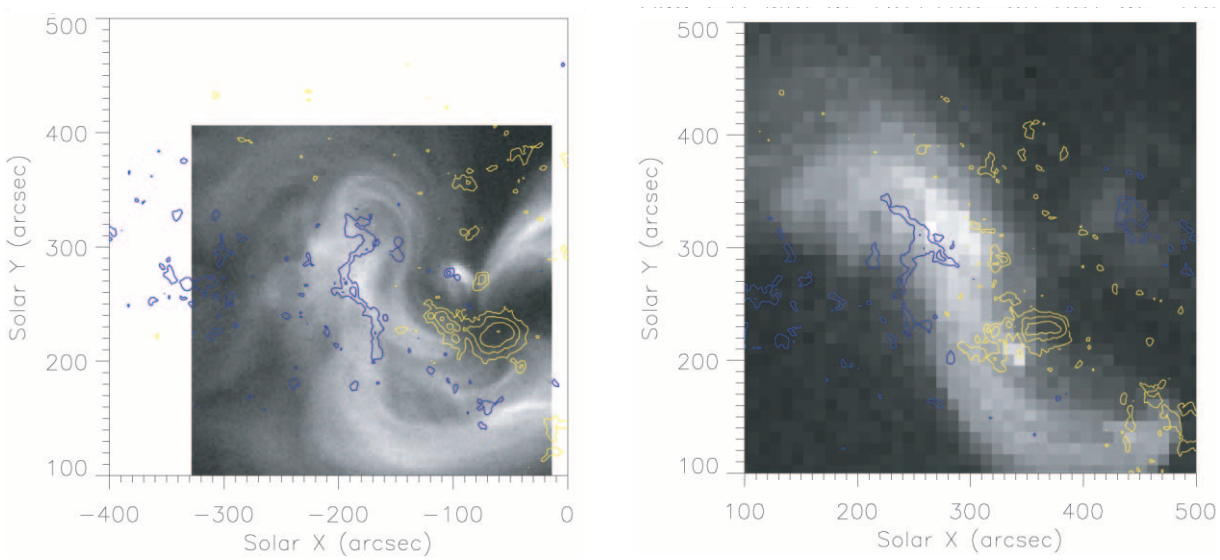

FIG. 6.—*Yohkoh*/SXT X-ray observations, with contours of MDI observations of magnetic field overlaid (*blue lines*: negative; *yellow lines*: positive), for 1999 August 19 (*left panel*) and August 21 (*right panel*).

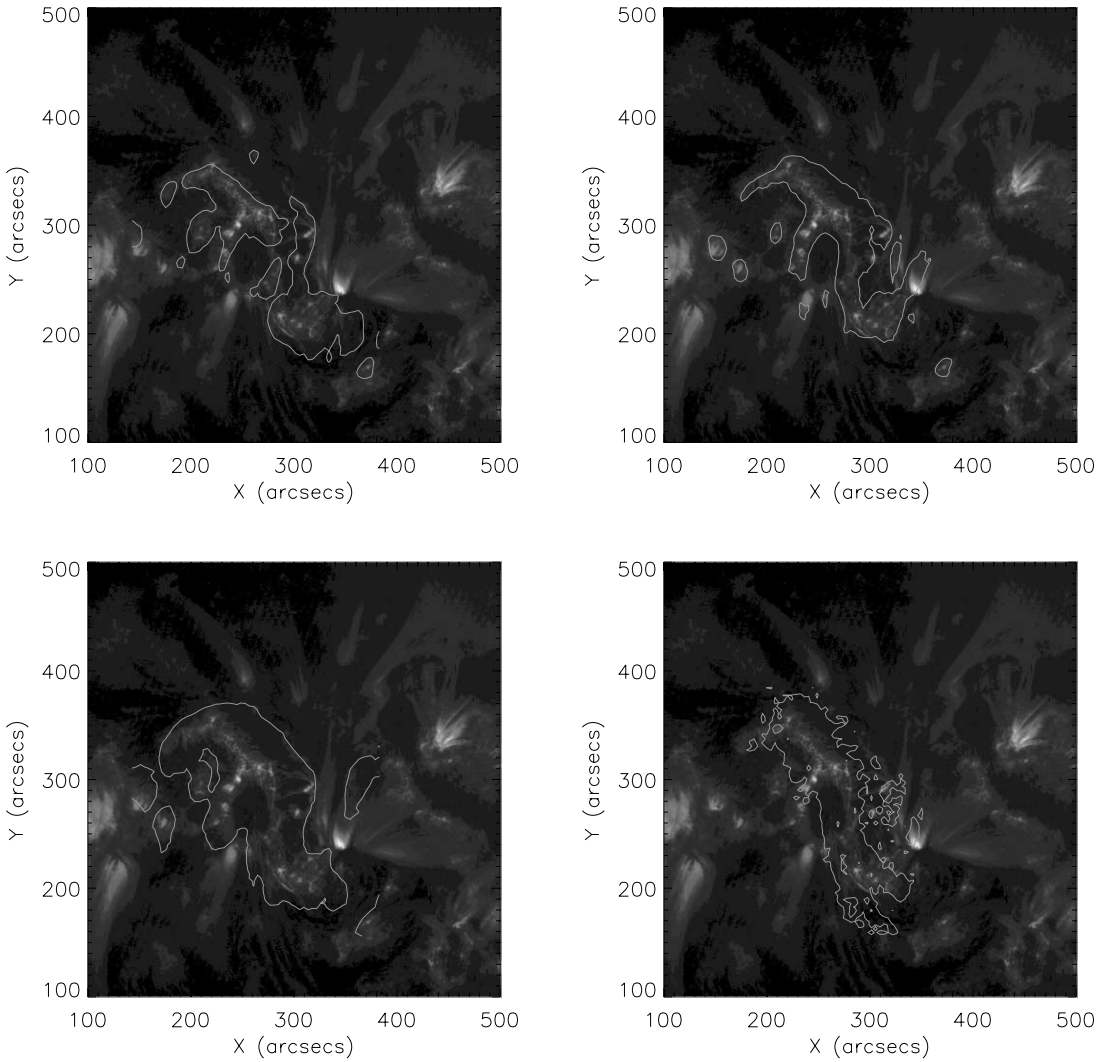

FIG. 7.—1999 August 21 18:21 UT: *TRACE* 171 Å EUV observations, with contours of CDS observations overlaid (*clockwise from upper left*: He I, Mg X, Fe XIX, and Si XII). [*See the electronic edition of the Journal for a color version of this figure.*]

One technique that allows us to model the three-dimensional magnetic structure of the entire sigmoidal region is an extrapolation of the photospheric field. We do so under the assumption that there are no significant currents perpendicular to the magnetic field and that any current parallel to the field can be parameterized with a single coefficient for the entire region (i.e., a linear force-free representation). This may not be a very good assumption for a region with such a complex structure, but it is an extrapolation possible using line-of-sight magnetic field observations and is a first step allowing us to consider how the field might vary with height as well as across AR 8668. In this manner, Figures 9*a*–9*d* show an extrapolation of photospheric magnetic field observations taken during the multiwavelength brightening of August 21. Note that the single parameter, α, has been chosen for this extrapolation in order to yield field lines that match the X-ray supersigmoid (*yellow lines*). The shorter blue loops were picked out as further inverse-S–shaped loops and match the location of the northerly subsigmoid. The different views of Figure 9 show that this blue subsigmoid lies below the yellow loops of the X-ray supersigmoid. A third set of loops that lies below both of these is also shown (*red lines*). These are in the area of the EFR and its associated AFS as described in § 2.2 and as seen in Figure 5. Note that the loops of the AFS oriented across the subsigmoid can also be seen in the *TRACE* images (Fig. 2*a*).

The identification of the upper, yellow magnetic loops with the *Yohkoh*/SXT supersigmoid and the lower, blue magnetic loops with the multiwavelength subsigmoid brightening is tempting, but we need to be careful. It is important to consider what exactly the different wavelengths are showing. We refer to short "loops" forming the basis of this brightening, but in fact not all of the wavelengths are showing loops—some are presumed to show only the footpoints of loops. Studies of *TRACE* observations have identified finely structured EUV emission at the level of the chromosphere/transition region, associated with overlying *Yohkoh*/SXT loops, which has been termed "moss" because of its intermittent, spongy appearance (Berger et al. 1999; Fletcher & De Pontieu 1999). Figure 7 shows *TRACE* observations at 171 Å, which primarily pick out the low-altitude (chromospheric) moss in the subsig-

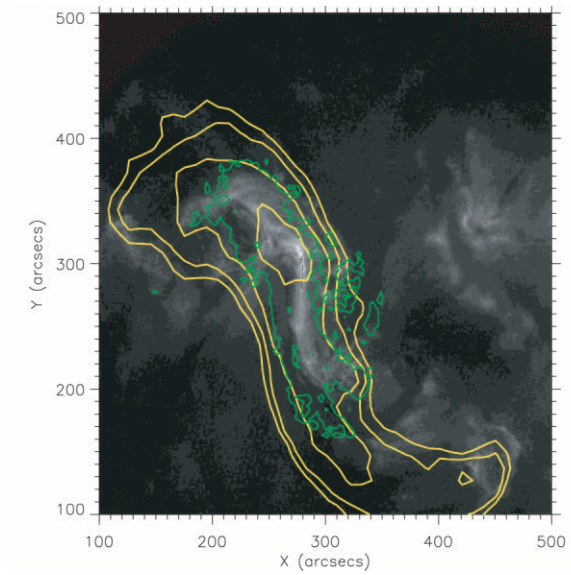

FIG. 8.—1999 August 21: *TRACE* 284 Å EUV observations, with contours of *Yohkoh*/SXT X-ray observations (*thick yellow lines*) and CDS Fe XIX (*thin green lines*) overlaid. Note that the CDS field of view is 4′ square and does not include the area containing the lower half of the supersigmoid brightening as seen by *Yohkoh*/SXT.

moid. The overlays of the *SOHO*/CDS lines imply that all but the hottest lines (Si XII, Fe XIX—sensitive to 2 million and 8 million K material, respectively) are mostly showing this moss. This is borne out by considering observations of the region at the west limb. (Although there is probably significant evolution between the multiwavelength brightening of August 21 and AR 8668 once it has reached the limb, the limb observations may still provide insight into the region's structure with height.) Figure 10*a* shows Mg X emission at the limb, overlaid with contours of Hα showing a prominence. Although there appears to be some higher altitude coronal emission in Mg X to the north, the brightest portion of the Mg X emission lies below the height of the prominence that can still be seen to the south. The emission coming from moss thus may generally overpower loop emission for the lines sensitive to material at about a million kelvins. This does not mean coronal loops do not exist at these temperatures. Although the brightest Mg X emission lies below the prominence, Figure 10 shows that loops to the north are still visible. But for the on-disk observations, it is only during transient brightenings such as on August 21 (e.g., Fig. 2) that the EUV emission shows loops that make up a clear sigmoidal pattern.

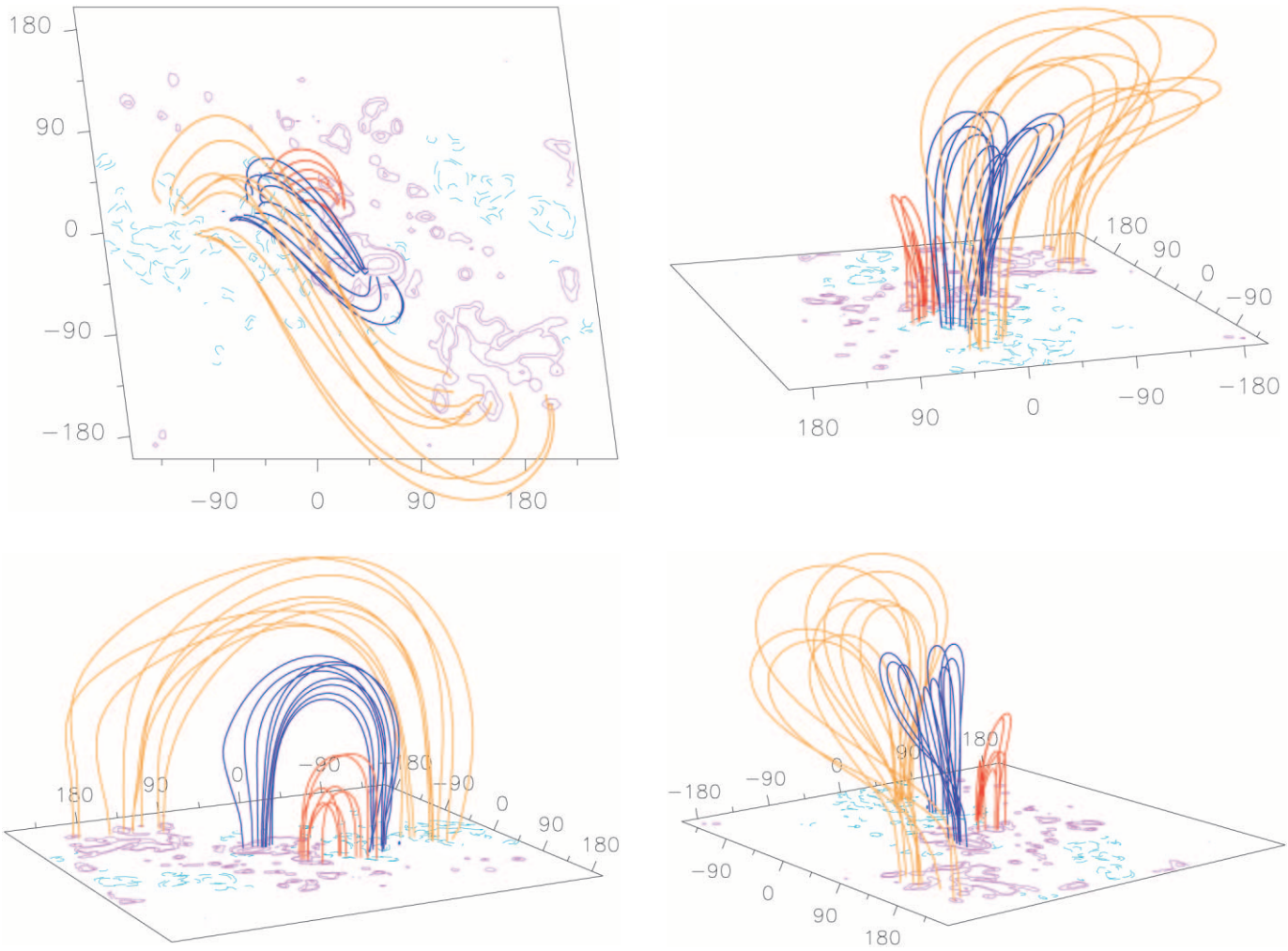

FIG. 9.—1999 August 21: Linear force-free extrapolation of MDI photospheric magnetic field. The three sets of colored lines highlight three sets of field lines, chosen as best matching the locations of the supersigmoid (*yellow lines*), subsigmoid (*blue lines*), and emerging flux region (*red lines*). The heights (Z) of the field lines have been adjusted slightly so that they can be more easily distinguished: $Z \rightarrow 20Z^{0.5}$. The four views plotted show four different viewing angles to illustrate the three-dimensional structure.

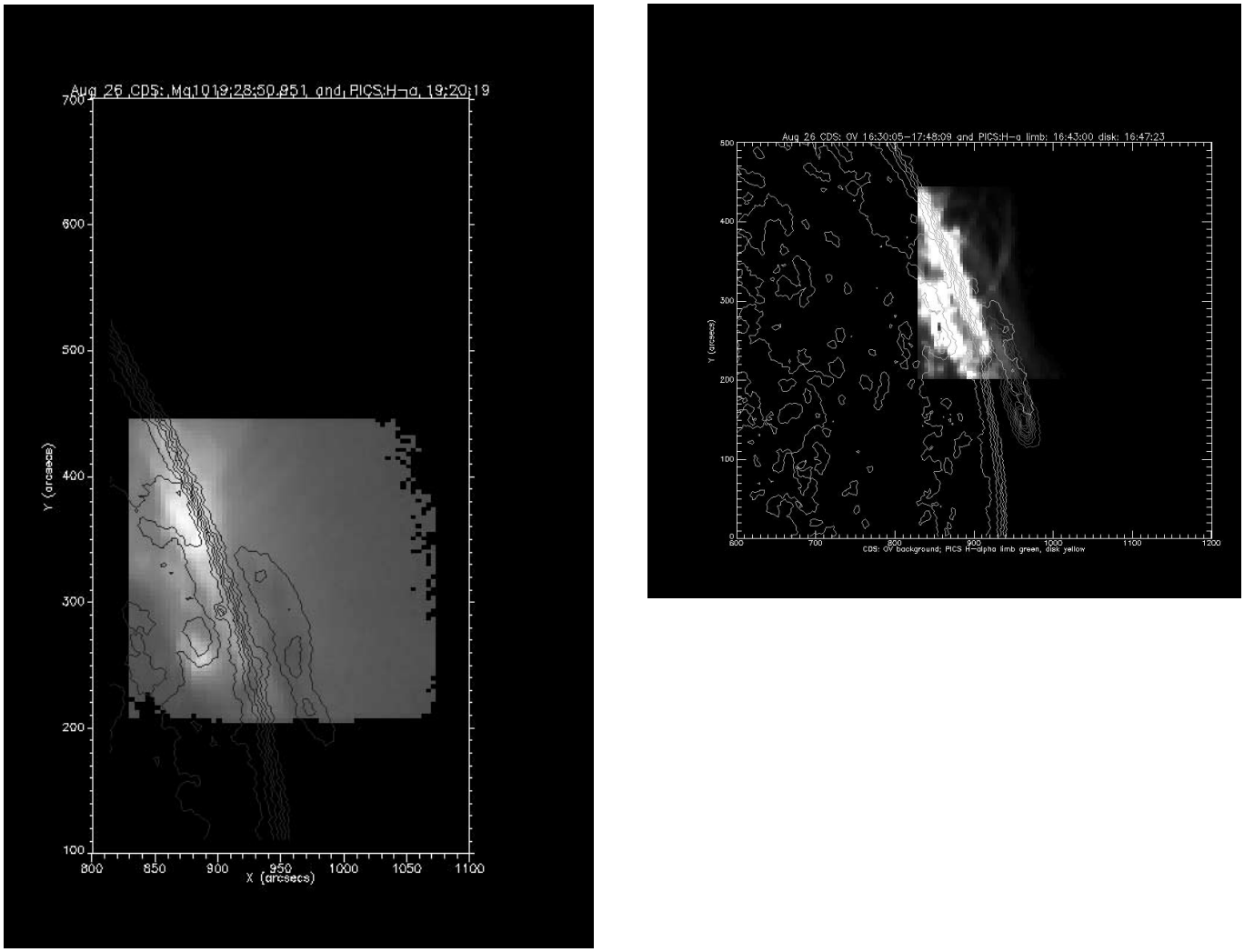

FIG. 10.—1999 August 26: Observations of AR 8668 at the west limb. *Left panel*: CDS Mg x emission (19:28 UT) with MLSO/PICS Hα contours overlaid (19:20 UT). *Right panel*: CDS O v emission (16:30 UT) with MLSO/PICS Hα contours overlaid (16:43 UT).

3.2. *Sigmoid Structure in Temperature, Density, and Velocity*

The temperature structure of AR 8668 can generally be determined by looking at which parts of the structure emit in which lines. Line ratio diagnostics can also be used to attempt to pin the temperature down more precisely. Del Zanna et al. (2002) considered *SOHO*/CDS temperature diagnostics of AR 8668 just prior to the August 21 multiwavelength brightening. The CDS lines did not show an obviously sigmoidal shape at this time, but more diffuse emission from Si XII and Fe XVI lines implied that some plasma of 2 million K temperature was present prior to the brightening, as is the case for most active regions. A lack of emission in Fe XIX implied that there was not much plasma at temperatures above a few million.

Although very little Fe XIX emission was present before the brightening, as the brightening began, a clear sigmoidal shape formed first in Fe XIX (Fig. 11). This implied heating to at least 8 million K. The fact that Fe XIX or any of the other *SOHO*/CDS lines did not show sigmoid loops prior to this implies that the X-ray sigmoid plasma had been at a temperature between 2 and 7 million K, since the *SOHO*/CDS lines used in this study lay either below 2 million K or above 7 million K. The small flarelike brightening (not *GOES* classified) centered on the EFR loops then appeared, and emission spread out from this brightening until a clear sigmoidal structure was lit up in the CDS lines. The hottest Fe XIX emission appeared as a sigmoid aligned with the supersigmoid seen in *Yohkoh*/SXT. The CDS field of view is only 4′ square and so shows the northern part of AR 8668. Thus, it is certainly possible that the Fe XIX emission shows the top half of this supersigmoid (Fig. 8). The cooler temperature lines (including *TRACE*) show the subsigmoid oriented at an angle to the supersigmoid. There is essentially a clockwise rotation between the sub- and supersigmoids, from cooler to hotter (Fig. 3).

We also analyzed plasma diagnostics from *SOHO*/CDS for the region once it had reached the west limb. Figure 12*a* shows the ratio of O V to O IV emission, a diagnostic sensitive to cooler [around $(1–3) \times 10^5$ K] material, while Figure 12*b* shows Fe XV/Mg XIX, a diagnostic sensitive to hotter [around $(1–3) \times 10^6$ K] material. From these we see that the hotter material lies above the cooler material, consistent with the magnetic field extrapolation where the supersigmoid loops lay above the subsigmoid.

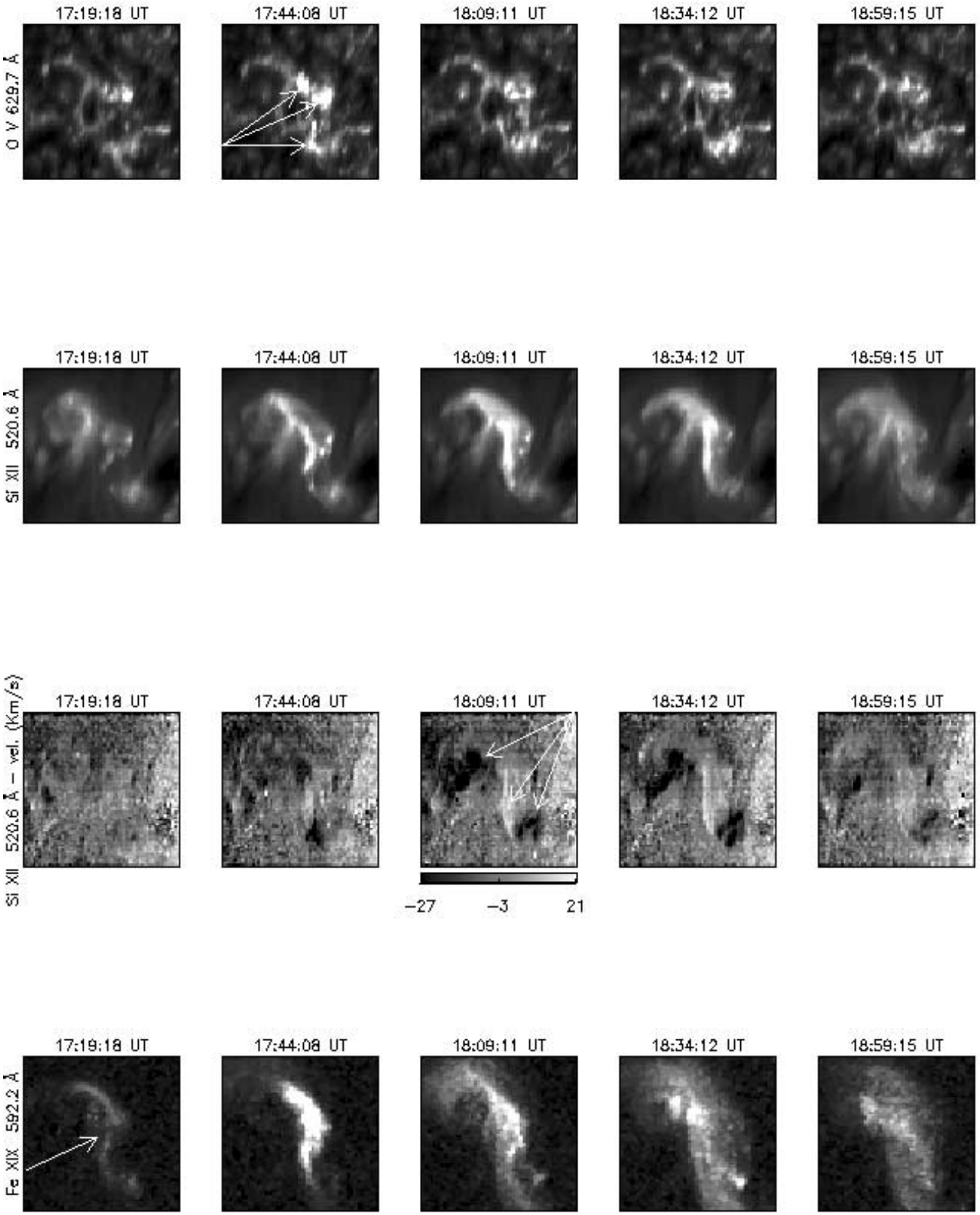

FIG. 11.—Sequence of CDS rasters, showing the subsigmoid brightening (not *GOES* classified) on August 21 17:44 UT. *Top to bottom*: Monochromatic images of O v (transition region) and Si xii (upper corona), velocity map as derived from Si xii line profiles (dark implies upflow), and images of the Fe xix line. All line intensity images in a row are plotted with the same intensity scale. The third row shows velocity maps, with the velocity scale in kilometers per second illustrated under the central image. The central time of each raster is indicated. Arrows point out the small flarelike brightening in the second O v raster, the downward (bright) and upward (dark) flows in the third Si xii velocity raster, and the sigmoidal precursor in the first Fe xix raster.

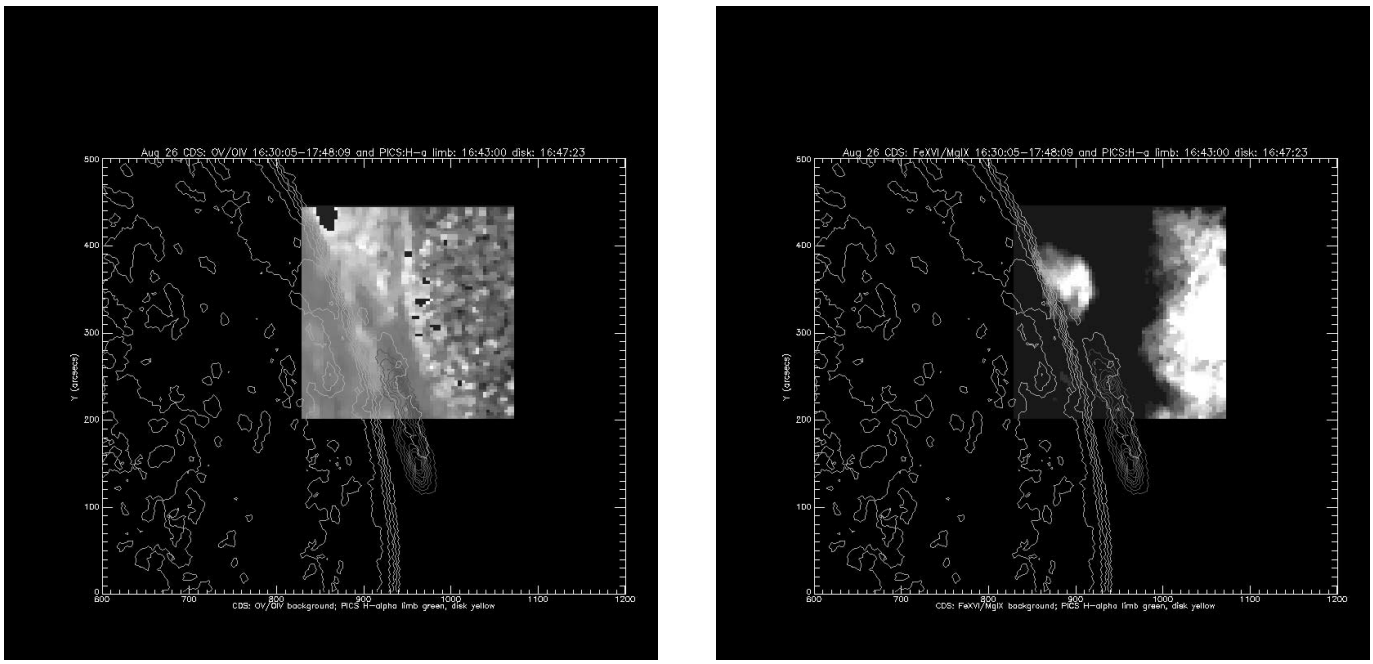

FIG. 12.—1999 August 26: Observations of AR 8668 at the west limb. *Left panel*: CDS O V/O IV temperature line ratio (cooler material) with MLSO/PICS Hα contours overlaid. *Right panel*: CDS Fe XVI/Mg IX temperature line ratio (hotter material) with MLSO/PICS Hα contours overlaid.

Velocities were also calculated during the August 21 event, showing significant (around 30 km s^{-1}) blueshift at both ends of the subsigmoid, implying upflow of 1–2 million K coronal plasma (Fig. 11, *third row*). Redshifts were also seen, implying downflow, primarily along the spine of the subsigmoid, both in coronal plasma and also to a lesser extent in cooler (O V line shifted) plasma. More downflow of material was seen at the ends of the subsigmoid in both coronal and transition region lines after the event. *TRACE* movies also show upflow and downflow of material during and after the event.

Densities were calculated prior to the brightening and were found to be in the range $(1–3) \times 10^{10}$ cm^{-3} for transition region values (from the O IV 629.9 Å/554.5 Å ratio) and about $(3 \pm 1) \times 10^9$ cm^{-3} for coronal temperatures (from the Si X 347.3 Å/356.05 Å ratio). The exception was in the region of the bright EFR loops, where densities reached 6×10^{10} cm^{-3}. During the sigmoidal brightening, densities greater than 10^{11} cm^{-3} were found using the O V/O IV line ratio. Finally, comparing diagnostic observations from just before and just after the event, Del Zanna et al. (2002) found that for the plasma around 1 million K there was no obvious change in overall densities and temperatures.

3.3. *Central Questions Raised by Observations and Analyses of Sigmoidal Structure*

These observations and analyses give us information about the sigmoidal region's structure in general and, in particular, during the August 21 multiwavelength brightening. This allows us to expand on some of our earlier questions, as well as to raise a couple of new ones and so continue our list of questions:

8. The magnetic field extrapolation used in § 3.1 was useful for getting an idea of how the observed X-ray and multiwavelength loop brightenings might relate to the field and to each other in three dimensions. However, it is a simple extrapolation using line-of-sight fields. How realistic a representation is it really? In particular, where does the filament fit into the magnetic field structure?

9. The brightening appeared in a range of wavelengths signifying material emitting at a range of temperatures. Many of these wavelengths showed a clear sigmoidal structure only during this brightening. (This was also the case found by Sterling et al. 2000; i.e., sigmoids generally appeared in EUV emission only during heightened activity such as flares.) Why were prebrightening sigmoidal structures only apparent in hot X-ray or cool filament temperatures? Either there were no sigmoidal loops present at EUV-emitting temperatures or any prebrightening EUV loop emission must have been very faint—so faint as to be generally not separately detectable against diffuse coronal emission from the surroundings and moss emission from below. Either way, the question is, what changed during the transient brightening on August 21 so that sigmoidal loops became visible in EUV?

10. Although a system of short loops connecting to the northerly positive pole appears to exist well before the transient brightening (e.g., Fig. 6*a*), during the brightening these loops have a distinctly sigmoidal and even tubelike appearance (Fig. 2). How does this subsigmoid magnetic structure relate to the overlying X-ray sigmoid and to the emerging magnetic flux that is observed before, during, and after the transient brightening?

11. *SOHO*/CDS observations showed that the small brightening, which preceded the appearance of the subsigmoid at multiple wavelengths and the velocity upflows, originated in the region of the new emerging magnetic flux (see, e.g., O V images of Fig. 11). In addition, an Fe XIX inverse-S–shaped precursor was visible possibly even before this EFR-centered brightening. What caused these three features (precursor, brightening, and upflows), and what might be the significance of their relative locations and timing?

12. What do the high transition region densities during the brightening imply?

13. Overlaying the emission from the various CDS lines observed during the brightening shows an apparent rotation of structure with wavelength/temperature, i.e., clockwise from cooler to hotter material (Fig. 3). Observations of the region at the limb and identification of structures with extrapolated magnetic field lines implies that the hotter material lies at higher altitudes; does this then mean that there is an overall twisting or shearing of the sigmoidal structure with height? Gibson et al. (1999a) reported evidence of a similar rotation with wavelength for a different sigmoidal region; in that case the rotation appeared counterclockwise from cooler to hotter material, but for a forward S rather than a backward S. Could this rotation of sigmoidal structure with temperature (and possibly height) be an indicator of the global direction of twist or magnetic helicity in the region?

4. INTERPRETATION

Let us now suggest one interpretation, describing the emergence, equilibration, and ultimate disruption of a twisted magnetic flux rope structure, against these observations. We do not claim this is the only possible explanation of the observations, but it does succeed at addressing the key questions of the observed sigmoidal structure and evolution—something any interpretation put forward needs to do. Questions that are so addressed are referred to in parentheses after the relevant points.

A twisted magnetic flux system emerges from beneath the photosphere into the corona forming the basis of AR 8668. We expect some minimum amount of preexisting twist in the magnetic structure as it emerges through the photosphere, for the following reasons: It has been found that a minimum amount of twist is needed to ensure that flux tubes rise cohesively through the convection zone (e.g., Emonet & Moreno-Insertis 1998; Fan, Zweibel, & Lantz 1998; Abbett, Fisher, & Fan 2000, 2001). Moreover, vector magnetogram observations imply that this twist is still there when magnetic structures emerge through the photosphere (e.g., Leka et al. 1996; Tanaka 1991). We would expect, however, that even if a magnetic structure similar to our highly simplified cartoon representation of Figure 13 exists subphotospherically, its form will probably be altered as it passes through the photosphere. For example, Fan (2001) showed using a numerical MHD simulation that the weight of entrained material in an emerging flux rope could stop it from smoothly rising into the corona intact. We therefore expect that the rising magnetic flux system will undergo significant alterations via reconnections as it moves into the corona. However, even though the magnetic field and associated currents would be altered by such reconnections, the magnetic helicity of the system must still be conserved (see Berger & Field 1984; Low 1994 for discussion of magnetic helicity conservation). As long as there is any helicity in the system at all, there must also be some currents and magnetic energy: this magnetic energy is essentially trapped by the conservation of magnetic helicity. (Please see Low 1996, 1999 for further discussion.) Note that we make the assumption that the helicity of our emerging magnetic structure stays more or less local to it, which is consistent with the observation that the sigmoidal structure is maintained. The flux rope thus undergoes reconnection within itself as well as reconnections with the external coronal field that it emerges into, until it has reached a metastable equilibrium state possessing a lowest possible energy that still conserves helicity. It is this equilibrium state that we represent as a twisted, ropelike structure (akin to a Slinky) suspended in the corona in Figure 13. (Question 1.)

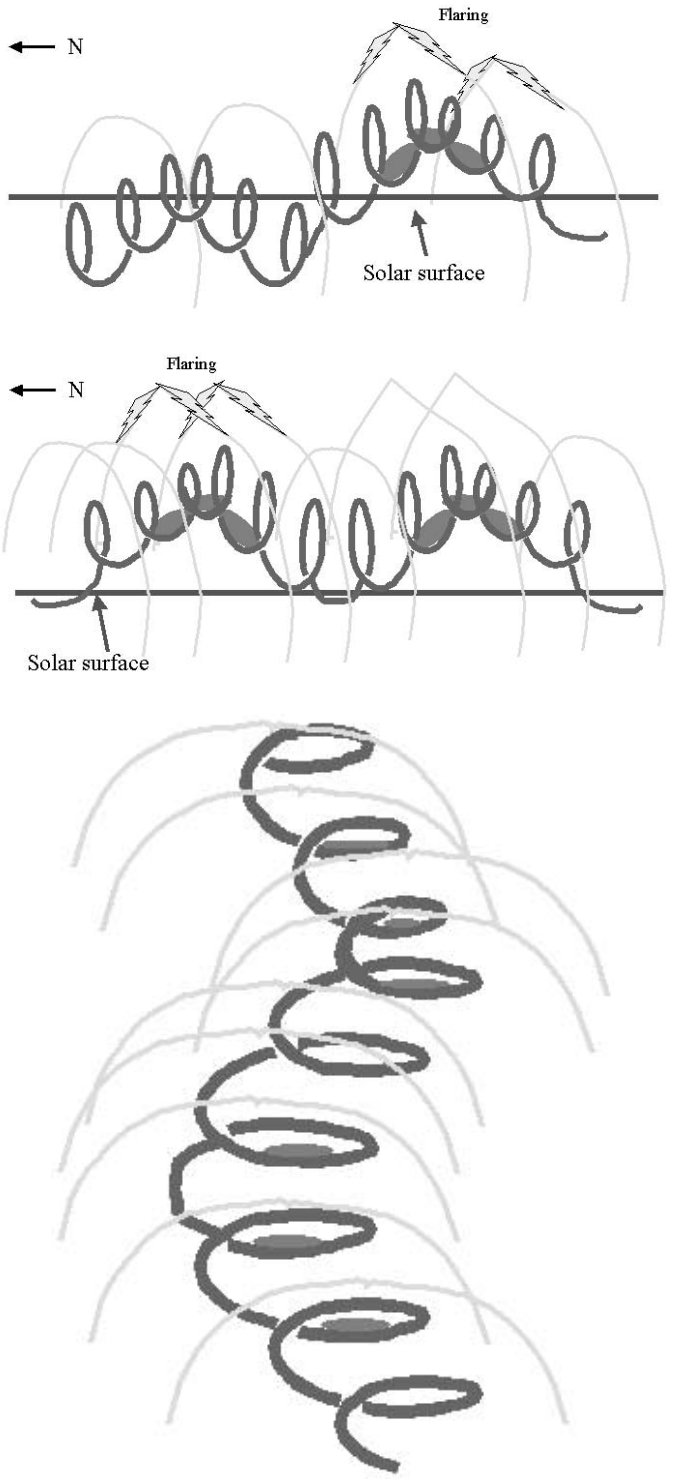

FIG. 13.—Cartoon representation of bent flux rope emerging through a solar surface. *Top panel*: Southern part of flux rope emerges, accompanied by flaring. *Middle panel*: Northern part of flux rope emerges, accompanied by flaring. *Bottom panel*: Same as middle, but viewed from above. Gray shading represents filament material. Note that this cartoon represents a highly twisted rope in order to emphasize its structure; the real system may contain a significantly smaller amount of twist (see discussion in text).

The observations of large flares and filament formation on August 16–17 are then the manifestation of the flux rope emerging, reforming, and equilibrating with its external environment. The sigmoid as seen in X-rays shows the interface between the field lines twisting around the rope axis and the external (nontwisting) fields (Fig. 13*c*) (B. C. Low & M. Berger 2002, in preparation). This is essentially a magnetic "separatrix," which generally refers to a surface across which the linkage of magnetic field lines is discontinuous. In classical electricity and magnetism theory, such surfaces in three dimensions originate from magnetic null points, from which field lines diverge. Quasi-separatrix layers (QSLs) extend this concept to refer to layers of finite thickness across which the field connectivity changes abruptly (Priest & Démoulin 1995; Démoulin et al. 1996a). These layers are the natural location for tangential discontinuities and current sheets to form during dynamic evolution of the system, where reconnection and dissipative heating can then arise (Parker 1987; Low 1991; Démoulin et al. 1996a). Therefore, we will refer to the X-ray sigmoid as a QSL occurring where neighboring field lines on either side have significantly different paths, leading to widely separated endpoints (i.e., winding vs. nonwinding lines). During its emergence and reformation, the rope expands upward against the external fields. The resulting heating from reconnections between tangentially discontinuous field lines illuminates the sigmoid QSL. Depending on the details of the rope versus external field topologies as well as the driver mechanism, this reconnection may lead to an explosive flare or, alternatively, yield a more gradual heating. Internal reconnections that act to reform the rope in the corona (such as that described in Démoulin et al. 1996b) also contribute to the overall sigmoidal shape. Reconnections along the surface layer and throughout the volume defined by the QSL continue until a minimum energy state is reached and an emerged (reformed) rope can exist in metastable equilibrium. Such equilibrating flares and brightenings are not necessarily indicative of a major ejection of the flux rope but rather may be reconnections acting to redistribute (but not remove) magnetic helicity within the system and dissipate as much energy as possible while conserving magnetic helicity. Thus, the basic geometry of the QSL (to first order an inverse-S–shaped surface) is largely unchanged throughout the region's disk passage and reappears whenever there is significant heating within and along the rope because of further reconnections as the rope evolves and is forced to form new equilibria with likewise evolving coronal conditions. (Questions 1, 2, and 3.)

The minimum energy configuration (i.e., flux rope) is a magnetic environment that can contain a filament—the filament material is supported by magnetic forces, as it sits in the dips that are the bottoms of the winds of the flux rope (Rust & Kumar 1994; Aulanier & Démoulin 1998; Gibson & Low 1998). Note that the magnetic field presented in Figure 9, most likely because of its simplicity as a linear force-free extrapolation of line-of-sight magnetic fields, does not yield a magnetic environment having dips that would support a filament. An extrapolation that uses a spatially varying force-free field parameter α and vector magnetogram observations of our sigmoidal region does show dipped magnetic field configurations, however (Y. Liu 2001, private communication). Nevertheless, neither extrapolation yields a highly wound structure as seen in our cartoon of Figure 13. Although the uncertainties in both the magnetic field observations and in the techniques used to extrapolate them mean we cannot rule out such a highly twisted structure, it has been argued that such a tightly wound flux rope is prone to instabilities and eruption: a stably existing rope may be more likely to contain significantly less twist (closer to one full turn; see, e.g., Rust & Kumar 1996). However, additional constraining effects such as the weight of filament mass within the rope could counteract this instability and allow a metastable equilibrium even for a highly wound structure. Thus, the presence of the high degree of twist would be an effective storage device for magnetic energy, and an eruption of the rope could easily be triggered if the filament weight were significantly altered, leading to a loss of equilibrium (see Low 1999). The degree of twist that could exist within CME precursors and the role of filament mass in CME energetics remain interesting open questions. (Questions 2 and 8.)

It is useful, for our interpretation of AR 8668, to consider the flux rope to have a bend in its middle (vs. height) and to have the southern part finish its equilibration with the background corona first (Figs. 13*a*–13*b*). The bend in the middle effectively keeps the northern and southern portions of the rope magnetically distinct until the full emergence (or reformation) of the rope: field lines are tied to the photosphere and so the two portions equilibrate with the external environment separately. (An interesting question that this provokes is how such a bend might arise—see, e.g., Linton et al. 1999; Fan et al. 1999 for a description of how the excitation of multiple unstable modes during a flux tube's convective rise through the photosphere produces compact kinks at a flux tube midpoint.) As the top of the flux rope pushes against the external field, reconnecting and flaring (Figs. 1*a* and 13*a*), the magnetic field structure in the southern part of the rope reaches a metastable equilibrium state where the filament can remain quiescently in bottoms of the winds of the southern part of the rope. The northern part of the rope lying above the photosphere is magnetically separate from the southern portion of the rope above the photosphere at this time and has not reached its own equilibrium yet—in the cartoon it has not itself fully emerged. As it does emerge, reform, and reach its own equilibrium, it also manifests the pattern of flaring followed by filament stabilization (Figs. 1*b* and 13*b*) corresponding to internal and external reconnections, followed by the appearance of a filament sitting in the bottoms of the reformed flux rope winds. The magnetic flux cancellation that occurs as the northern part of the filament stabilizes (Fig. 4) might be interpreted as the actual emergence of the central bend of the flux rope, as the U-shaped bottoms of the magnetic flux rope manifest as an apparent magnetic flux cancellation (see Fig. 13*b* and Spruit, Title, & van Ballegooijen 1987; Low 1996; van Driel-Gesztelyi, Malherbe, & Démoulin 2000). Another interpretation, consistent with the idea that the rope is reforming in the atmosphere, was presented by Chae et al. (2000), who cited AR 8668 BBSO Hα observations of diverging flows and upflows of cool mass at the location of the magnetic flux cancellation as evidence of an ongoing reconnective process (van Ballegooijen & Martens 1989) and an associated upward transport of filament material (Rust & Kumar 1994). It is possible that the stretching caused by upward expansion of the top of the flux rope has led to a reconnection across the dipped magnetic field lines weighed down by photo-

spheric material, with a subsequent lifting of a lighter load of filament material into the corona. (Questions 2 and 4.)

The flares of August 16 and 17 are thus stabilizing rather than destabilizing effects on the flux rope and its associated filament. Although on August 17 there is a clear sigmoid-to-cusp transition above the northern part of the filament channel and associated postflare loops, there is no clear evidence that filament material is ejected; in fact, the northern part of the filament becomes clear immediately after this flare (see also Pevtsov 2002). We interpret this to mean that this flare, like the others on August 16 and 17, is part of the equilibration process—if any of the flux rope erupts, it does so only partially and in a manner that leaves the rest of the flux rope behind in a metastable equilibrium allowing the filament to continue to grow (see, e.g., Tang 1986 and Fig. 3 of Gilbert et al. 2001). However, the neighboring streamer/polar crown filament does erupt in a large CME. This is not surprising, since the equilibration between AR 8668 and surrounding fields affects the configuration of the external field as well as that of AR 8668 (an interesting analysis of how emerging magnetic flux at a given latitude can cause CMEs to erupt at a significantly removed latitude can be found in Zhang & Low 2001). Conceivably, the streamer to the northeast may have been in an energetic state, ready to erupt, so that the first August 17 flare in AR 8668 (with a peak at 13:23 UT) provides perturbation enough to trigger it. The second flare (with a peak at 16:02 UT) and X-ray cusp formation shows the magnetic field reconnecting behind that CME and/or perhaps a partial ejection of the flux rope of AR 8668. The flux rope is then left in metastable equilibrium. (Questions 2 and 5.)

The rope is now in a relatively stable, presumably minimum energy configuration (for a given magnetic helicity), and the filament continues to grow. This is the observed behavior of August 18–19. At the same time, the X-ray sigmoid is less evident, since the system is relaxed and no longer reconnecting much within itself or with its environment, and so the QSL is only minimally heated (although the QSL still exists and presumably still has a sigmoidal shape). Thus, the X-ray sigmoid is apparent during the activity associated with equilibration between the flux rope and coronal environment, and the filament is at its most apparent during the resulting metastable equilibrium state. During this period, however, motion in the southern part of the sigmoidal filament increases, until on August 20 the southern part of the filament completely disappears. It is possible that it is at least partly ejected, taking with it a portion of the flux rope's stored-up magnetic helicity. It is interesting to note that the dimming seen by *SOHO*/EIT precedes the disappearance of the southern part of the filament; this might imply that the overlying coronal arcades open up, removing a necessary constraint on the region's metastable equilibrium, so that the flux rope then erupts outward. The entire flux rope is not ejected, however, and the northern portion of the filament remains. By the morning of August 21, the northern part of the filament also disappears (possibly in another partial ejection). New magnetic flux is observed to emerge near the filament's midpoint prior to the disappearance of the upper portion of the inverse-S–shaped filament. Such emerging flux may significantly affect the lower boundary condition of the original flux rope, and in so doing redefine what is a minimum energy for the system, or in some other manner destabilize the rope (see, e.g., Raadu et al. 1988). The effect of the emerging flux, along with the lightening of the gravitational anchor of the southern part of the filament as well as the possible ejection of some of the rope's helicity with the southern part of the filament, may be the key factors in completely pushing the flux rope out of its metastable equilibrium. (Questions 3 and 6.)

As these effects push the system once again into a period of instability, the X-ray sigmoid structure is at its most obvious. It is at this point also that the subsigmoid becomes temporarily apparent at a range of wavelengths. We interpret this subsigmoid brightening to arise because of tangential discontinuities and reconnections along the QSL that lies between the bottom of the original flux rope and the new EFR that pushes up from below. The first manifestation of the multiwavelength brightening is the appearance in Fe XIX of a sigmoidal structure, aligned, however, with the *Yohkoh*/SXT supersigmoid. The Fe XIX precursor may indicate heating along the upper QSL, as the original flux rope is pushed up against the external fields by the emerging flux below. The small brightening is then visible at the subsigmoid QSL centered on the EFR, and velocity upflows are observed at the endpoints of the subsigmoid. The subsigmoid begins to appear at a range of temperatures because the flarelike heating has caused chromospheric evaporation of enough material to coronal heights so that enhanced emission can be observed at a range of temperatures along the subsigmoid QSL. Specifically, chromospheric material is evaporated, causing the upflows observed by *SOHO*/CDS (see also Czaykowska et al. 1999). At the same time, some cools down and falls back down (*SOHO*/CDS redshifts) and in so doing increases transition region densities. The increase of density in the subsigmoid loops means that there is enough material there to be seen at 1–2 million K as the flare-heated plasma cools down. The supersigmoid, however, never shows up brightly at wavelengths other than the very hottest because it is both longer and higher than the subsigmoid, so that the density of evaporated material at 1–2 million K is much less. Such an inverse relationship between brightness and loop length during flare activity has been observed both for sigmoidal and nonsigmoidal loops (Manoharan et al. 1996; Gaizauskas et al. 1998; Mandrini et al. 1996). Thus, sigmoids may not be generally apparent at wavelengths other than soft X-ray because ordinarily there is not enough material at EUV temperatures in the sigmoidal loops to be easily visible, particularly against the strong background EUV emission from chromospheric moss. Because *SOHO*/CDS and *TRACE* happened to be observing during the flare and with a high time cadence, they caught the brightening of the subsigmoid at a range of wavelengths while densities in the subsigmoid were high. The supersigmoid is apparent both before, during, and after the subsigmoid brightening at soft X-ray temperatures, because enough plasma is sustained at soft X-ray temperatures to show up easily against an otherwise dark background. However, note that the supersigmoid is most clear during the brightening, as it too responds to the input of energy from the small flare. (Questions 3, 7, 9, 10, 11, and 12.)

We have not explicitly modeled the magnetic configuration of our flux rope and the QSL associated with it. One possible topology has been presented by Titov & Démoulin (1999). This model predicts upper and lower QSLs, akin to the observed sub- and supersigmoids. Work is being undertaken elsewhere (R. C. Canfield et al. 2002, in preparation) to explicitly compare predictions of the Titov & Démoulin (1999) model to observations of AR 8668. However, the

Titov & Démoulin (1999) topology does not include or require the EFR for the appearance of the lower QSL. Observations of the multiwavelength subsigmoid brightening of August 21 imply that the small flare that triggered the brightening is located at the EFR. It is possible that the lower QSL existed throughout the disk passage of AR 8668 (note, for example, the lower loops visible on August 19 in Fig. 6*a*) and that the role of the EFR pushing up from underneath is primarily squeezing magnetic fluxes together, causing tangential discontinuities in the field and subsequent reconnections along the rope's QSLs. It may in the process transfer some of its helicity to the flux rope above it, so that the lower QSL takes on a clearly sigmoidal appearance. We have analyzed vector magnetogram observations from the Huairou solar observing station and found that they indicate the same sign (negative) of current helicity for the original sigmoidal fields and the EFR (the method to calculate the helicity and the definition of the sign of the helicity are as described in Abramenko, Wang, & Yurchison 1996; as defined in that paper, the imbalance ρ of current helicity is -21% for AR 8668 as a whole, -29% for the central positive polarity [sunspot], and -21% for the emerging flux region). Thus, the emergence of the new magnetic flux could add to the twist in the original flux rope (see, e.g., Canfield & Reardon 1998; Moore & Roumeliotis 1992) and so compensate for magnetic helicity lost in the ejection of pieces of the filament. Indeed, the apparently separate magnetic flux systems of the original flux rope and the EFR could actually be two outbreaks of a single complex subphotospheric flux rope. The twisting of the combined system with height as seen by the *SOHO*/CDS lines in Figure 3 may be a result of the single shared direction of twist (for example, such a rotation of field lines with height was described for a CME spheromak-type flux rope model in Gibson & Low 2000). (Questions 1, 10, and 13.)

As a final comment, we note the almost too apt symmetry of the evolution of our sigmoidal region. It appears to be in a process of formation as it first becomes visible in the eastern hemisphere; then, at central meridian, the filament is at its largest and most stable; and then, as it moves toward the western limb, it loses stability and decays. We seem to witness birth, maturity, and death. Although ultimately every active region does go through these three stages, we do not necessarily think that the full process was viewed in the disk passage of AR 8668. Rather, the evolution of the system was more of a binary one, alternating between stability and the activity necessary for its reequilibration. As new flux emerged and the global coronal field evolved, the metastable equilibrium was disrupted, and the region went through brightenings and eruptions until once again stability was obtained (note the lack of flares/brightenings and eruptions on August 22–25). It is impossible to definitely say whether the region is still sigmoidal when it has reached the limb, since projection rules out an X-ray sigmoid identification. However, the fact that the region is still active (as evidenced by the jet of August 26) implies that the region still may have energy stored up in magnetic helicity and be going through another phase of equilibrating with its environment. (Question 3.)

5. CONCLUSIONS

The observations outlined in this paper represent the most comprehensive study to date of a sigmoidal active region. By considering observations at multiple wavelengths that span the full passage of the region across the solar disk, we have gained new insight into the structure and evolution of sigmoids and encapsulated the outstanding issues raised by observations into a list of physical questions that need to be addressed in any theoretical interpretation.

One such question is raised by the observation that a clear S shape is generally visible only in the very hot X-ray images or the relatively cool Hα filament images but does appear at 1–2 million K during events such as the August 21 brightening. We suggest that this hinges on the density in the loops: when chromospheric evaporation supplies enough hot, dense material to the short loops of the subsigmoid region, these become visible in intermediate temperatures as they cool down. The supersigmoid remains largely invisible in the intermediate temperature plasma, since an equivalent energy input yields a much lower density in the high, long loops. In between flares or flarelike brightenings, slow or bursty reconnection heating may not be energetic enough to evaporate sufficient material to any of the sigmoidal loops for 1–2 million K plasma to appear against its background emission, and so only the X-ray sigmoid can appear, since a significantly lower density may be adequate for X-ray loops to be visible against their relatively dark background.

The hypothesis that a sigmoid's manifest twist leads to a region likely to erupt is borne out by the observations. We have presented an interpretation of the sigmoid's evolution as the emergence of a flux rope, where the filament rests within the bottom of the winds of the rope and the X-ray supersigmoid appears at the quasi-separatrix layer between the rope and external fields. As new emerging flux pushes up underneath the original flux rope, a subsigmoid appears at the QSL between the emerging flux and the supersigmoid. Various flares and brightenings are common at these QSLs, but the energy stored in the twist of the flux rope is not shed during these dissipative events, and so the flux rope structure is not greatly changed (as is directly implied by the observed lack of change in density and temperature after the August 21 brightening). The primary mechanism for ultimately shedding the sigmoid's twist and its associated energy may well be bodily ejection into interplanetary space by a CME (Low 1994), but there is no evidence in our observations of the complete ejection of the flux rope structure; rather, it appears that the rope undergoes multiple partial ejections as reconnections release one piece at a time (Tang 1986; Gilbert et al. 2001). Emerging magnetic flux also continues to input magnetic helicity into the region. This has been discussed for the easily identified EFR associated with our region on and after August 21 but could also occur as tiny EFRs with associated twist transfer their helicity from their own smaller scale to the larger scale of the sigmoid flux rope: MHD turbulence tends to drive magnetic helicity from small to large scales. Thus, the paradox of the sigmoid being both active and robustly recurrent is resolved: it is intrinsically energetic in its interaction with its surroundings but not itself easy to destroy since the helicity that maintains its sigmoidal interface is continually replenished via emerging magnetic flux and only partially removed through ejections.

Of course, our interpretation does not succeed in explaining all of the observed behavior of AR 8668 and, indeed, has raised many questions that are incentives for future studies. For example, we have described the filament material as stably resting in the bottoms of winds of a Slinky-type flux

rope, but observations show material moving back and forth along the axis of the filament. This might be explained in terms of a sloshing back and forth of the flux rope (and so an apparent axial motion of material that actually does not move out of its local "dip") but may also point to a steady state of the filament where material is in constant motion along the filament, in and out of local dipped regions of the magnetic field. (See Gilbert et al. 2001 for an interpretation of apparent helical motions along a filament [consistent with a flux rope model] and Karpen et al. 2001 for a discussion of whether dipped fields are necessary in a dynamic filament environment.) Further analysis of observed filament velocities for AR 8668 might clarify this issue.

In conclusion, we feel that we have presented a physical interpretation that successfully addresses enough of the observed phenomena to make it plausible and crucially allows us to step back from the details of the observations and view the fundamental processes that they illustrate.

We would like to acknowledge the following people and sources: B. C. Low for helpful discussions, Y. Fan for internal NCAR review of the paper, Y. Guo for assistance with the BBSO data, S. Martin and P. Zink for comments during the WSM3 campaign, the *SOHO*/CDS team, and the LASCO daily movie page.[12] The *Yohkoh*/SXT project is a collaborative project of Lockheed-Martin Solar and Astrophysics Laboratory (LMSAL), the National Astronomical Observatory of Japan, and the University of Tokyo, supported by NASA and ISAS. *TRACE* is operated jointly out of Goddard Space Flight Center by scientists from the University of Chicago, Montana State University, LMSAL, and the Harvard-Smithsonian Center for Astrophysics. *SOHO* is a project of international cooperation between ESA and NASA. Part of S. E. G.'s work was done while visiting the Department of Applied Mathematics and Theoretical Physics at the University of Cambridge. L. F. acknowledges support from NASA grants NAS8-37334 (SXT) and NAS5-38099 (*TRACE*) and from a PPARC Standard Astronomy Grant. H. E. M. and G. D. Z. also acknowledge financial support from PPARC. C. H. M. acknowledges support from the Carrera del Investigador Científico, CONICET, Argentina. C. H. M., P. D., and B. S. acknowledge financial support from ECOS (France) and SETCIP (Argentina) through their cooperative science program (A01U04). We would also like to thank the referee for valuable comments on this paper.

[12] Available at http://lasco-www.nrl.navy.mil/daily_mpg.

REFERENCES

Abbett, W., Fisher, G. H., & Fan, Y. 2000, ApJ, 540, 548
———. 2001, ApJ, 546, 1194
Abramenko, V. I., Wang, T., & Yurchison, V. B. 1996, Sol. Phys., 168, 75
Aulanier, G., & Démoulin, P. 1998, A&A, 329, 1125
Aurass, H., Vrsnak, B., Hofmann, A., & Rudzjak, V. 1997, Sol. Phys., 174, 91
Berger, M., & Field, G. 1984, J. Fluid Mech., 147, 133
Berger, T. E., De Pontieu, B., Fletcher, L., Schrijver, C. J., Tarbell, T. D., & Title, A. M. 1999, Sol. Phys., 190, 409
Biesecker, D. A., et al. 1999, J. Geophys. Res., 104, 9679
Canfield, R. C., Hudson, H. S., & McKenzie, D. E. 1999, Geophys. Res. Lett., 26, 627
Canfield, R. C., & Reardon, K. P. 1998, Sol. Phys., 182, 145
Chae, J., Denker, C., Spirock, T. J., Wang, H., & Goode, P. R. 2000, Sol. Phys., 195, 333
Czaykowska, A., De Pontieu, B., Alexander, D., & Rank, G. 1999, ApJ, 521, L75
Del Zanna, G., Gibson, S. E., Mason, H. E., Pike, C. D., & Mandrini, C. H. 2002, Adv. Space Res., in press
Démoulin, P., Hénoux, J. C., Priest, E. R., & Mandrini, C. H. 1996a, A&A, 308, 643
Démoulin, P., Priest, E. R., & Lonie, D. P. 1996b, J. Geophys. Res., 101, 7631
Emonet, T., & Moreno-Insertis, F. 1998, ApJ, 492, 804
Fan, Y. 2001, ApJ, 554, L111
Fan, Y., Zweibel, E. G., & Lantz, S. R. 1998, ApJ, 493, 480
Fan, Y., Zweibel, E. G., Linton, M. G., & Fisher, G. H. 1999, ApJ, 521, 460
Fletcher, L., & De Pontieu, B. 1999, ApJ, 520, L135
Gaizauskas, V., Mandrini, C. H., Démoulin, P., Luoni, M. L., & Rovira, M. G. 1998, A&A, 332, 353
Galvin, A. B., & Kohl, J. 1999, J. Geophys. Res., 104, 9673
Gibson, S. E., & Low, B. C. 1998, ApJ, 493, 460
———. 2000, J. Geophys. Res., 105, 18187
Gibson, S. E., Mason, H. E., Pike, C. D., & Young, P. R. 1999a, 8th SOHO Workshop (ESA SP-446; Noordwijk: ESA), 331
Gibson, S. E., et al. 1999b, ApJ, 520, 871
Gilbert, H. R., Holzer, T. E., Low, B. C., & Burkepile, J. T. 2001, ApJ, 549, 1221
Glover, A., Ranns, N. D. R., Harra, L. K., & Culhane, J. L. 2001, Geophys. Res. Lett., 27, 2161
Harrison, R. A., et al. 1995, Sol. Phys., 162, 233
Hudson, H. S., Lemen, J. R., St. Cyr, O. C., Sterling, A. C., & Webb, D. F. 1998, Geophys. Res. Lett, 25, 248
Karpen, J. T., Antiochos, S. K., Hohensee, M., Klimchuk, J. A., & Macniece, P. J. 2001, ApJ, 553, L85
Leka, K. D., Canfield, R. C., McClymont, A. N., & van Driel-Gesztelyi, L. 1996, ApJ, 462, 547
Linton, M. G., Fisher, G. H., Dahlburg, R. B., & Fan, Y. 1999, ApJ, 522, 1190
Lites, B. W., & Low, B. C. 1997, Sol. Phys., 174, 91
López Fuentes, M. C., Démoulin, P., Mandrini, C. H., & van Driel-Gesztelyi, L. 2000, ApJ, 544, 540
Low, B. C. 1991, ApJ, 381, 295
———. 1994, Phys. Plasmas, 1, 1684
———. 1996, Sol. Phys., 167, 217
———. 1999, in AIP Conf. Proc. 471, Solar Wind Nine, ed. S. R. Habbal, R. Esser, J. V. Hollweg, & P. A. Isenberg (Woodbury: AIP), 109
Mandrini, C. H., Démoulin, P., van Driel-Gesztelyi, L., Schmieder, B., Cauzzi, G., & Hofmann, A. 1996, Sol. Phys., 168, 115
Manoharan, P. K., van Driel-Gesztelyi, L., Pick, M., & Démoulin, P. 1996, ApJ, 468, L73
Moore, R. L., & Roumeliotis, G. 1992, in Eruptive Solar Flares, ed. Z. Svestka, B. V. Jackson, & M. E. Machado (Lecture Notes in Physics 399; Berlin: Springer), 69
Moore, R. L., Sterling, A. C., Hudson, H. S., & Lemen, J. R. 2001, ApJ, 552, 833
Parker, E. N. 1987, ApJ, 318, 876
Pevtsov, A. A. 2002, Sol. Phys., in press
Pevtsov, A. A., & Canfield, R. C. 1999, Geophys. Monogr., 111, 103
Pevtsov, A. A., Canfield, R. C., & Zirin, H. 1996, ApJ, 473, 533
Priest, E. R., & Démoulin, P. 1995, J. Geophys. Res., 100, 23443
Raadu, M. A., Schmieder, B., Mein, N., & Gesztelyi, L. 1988, A&A, 197, 289
Rust, D. M., & Kumar, A. 1994, Sol. Phys., 155, 69
———. 1996, ApJ, 464, L199
Spruit, H. C., Title, A. M., & van Ballegooijen, A. A. 1987, Sol. Phys., 110, 115
Sterling, A. C., & Hudson, H. S. 1997, ApJ, 491, L55
Sterling, A. C., Hudson, H. S., Thompson, B. J., & Zarro, D. M. 2000, ApJ, 532, 628
Tanaka, K. 1991, Sol. Phys., 136, 133
Tang, F. 1986, Sol. Phys., 105, 399
Thompson, B. J., St. Cyr, O. C., Plunkett, S. P., Gurman, J. B., Hudson, H. S., Howard, R. A., & Michels, D. J. 1999, Geophys. Monogr., 109, 31
Titov, V. S., & Démoulin, P. 1999, A&A, 351, 707
van Ballegooijen, A. A., & Martens, P. C. 1989, ApJ, 343, 971
van Driel-Gesztelyi, L., Malherbe, J.-M., & Démoulin, P. 2000, A&A, 364, 845
Wang, H., et al. 2000, ApJ, 536, 971
Zarro, D. M., Sterling, A. C., Thompson, B. J., Hudson, H. S., & Nitta, N. 1999, ApJ, 520, L139
Zhang, M., & Low, B. C. 2001, ApJ, 561, 406